In presenting the dissertation as a partial fulfillment of the requirements for an advanced degree from the Georgia Institute of Technology, I agree that the Library of the Institute shall make it available for inspection and circulation in accordance with its regulations governing materials of this type. I agree that permission to copy from, or to publish from, this dissertation may be granted by the professor under whose direction it was written, or, in his absence, by the Dean of the Graduate Division when such copying or publication is solely for scholarly purposes and does not involve potential financial gain. It is understood that any copying from, or publication of, this dissertation which involves potential financial gain will not be allowed without written permission.

_____

_____

7/25/68

ELECTRICAL CONDUCTIVITY OF SEEDED GASES AT MODERATE TEMPERATURES

A THESIS

Presented to

The Faculty of the Graduate Division

by

Mack Wayne Dowdy

In Partial Fulfillment

of the Requirements for the Degree

Doctor of Philosophy

in the School of Mechanical Engineering

Georgia Institute of Technology

December 1968

ELECTRICAL CONDUCTIVITY OF SEEDED GASES

AT

MODERATE TEMPERATURES

Approved:

Chairman

Date approved by Chairman: 12/13/65

ACKNOWLEDGMENTS

The author would like to express sincere appreciation to the many people who have encouraged him throughout his life, especially to his wife, Delores, whose love and understanding have helped sustain him through graduate school.

The author is very grateful to Dr. Walter O. Carlson, the faculty advisor for this thesis, for his encouragement and advice throughout the course of this work. The constructive comments and the time devoted to this thesis by the other members of the reading committee, Dr. John W. Hooper and Dr. James C. Wu, are gratefully acknowledged. The author would also like to thank Messrs. C. R. Bannister, L. A. Cavalli, R. J. Collins, J. G. Doyle, J. W. Davis and D. W. Kiebel for their help in fabricating the experimental apparatus.

A special note of thanks is due Bill Flegal whose help in all the experimental tests was very valuable.

TABLE OF CONTENTS

LIST OF TABLES

LIST OF ILLUSTRATIONS

NOMENCLATURE

A	cross-sectional area of test section
$A_{j\to o}$	Einstein spontaneous emission probability for transition from the j^{th} excited state to the ground state
$\vec{B}$	magnetic induction
c	speed of light
e	electronic charge
E_A	function defined by Equation (10)
E_K	function defined by Equation (11)
$\vec{E}$	electric field
$\vec{E}^*$	electric field in the "rest frame" of the gas
$f_{1\to o}$	emission oscillator strength of the $4P_{1/2}$ excited state
$f_{2\to o}$	emission oscillator strength of the $4P_{3/2}$ excited state
F	potassium seeding fraction
g_o	statistical weight of the ground state
g_j	statistical weight of the j^{th} excited state
$\vec{g}$	relative velocity between two colliding particles
G_j	resonance escape factor
h	Plank's constant
$h\nu_j$	energy of transition from the j^{th} excited state to the ground state
I	total current passing through the test section
j	current density
k	Boltzmann's constant
ℓ	distance between the two voltage probes

m_A mass of an argon atom

m_e mass of an electron

$\dot{m}_A$ mass flow rate of argon

$\dot{m}_K$ mass flow rate of potassium

$\tilde{M}_A$ molecular weight of argon

$\tilde{M}_K$ molecular weight of potassium

n_A number density of argon atoms

n_e number density of electrons

n_i number density of ions

n_j number of density of atoms in the j^{th} excited state

n_K number density of potassium atoms

n_o number density of atoms in the ground state

n_s number density of s species

n_A^+ number density of argon ions

n_K^+ number density of potassium ions

n_K^o number density of potassium atoms in the ground state

n_K^1 number density of potassium atoms in the $4P_{1/2}$ excited state

n_K^2 number density of potassium atoms in the $4P_{3/2}$ excited state

P gas pressure

P_A^{int} internal partition function for argon atoms

$P_{A^+}^{int}$ internal partition function for argon ions

P_e^{int} internal partition function for electrons

P_K^{int} internal partition function for potassium atoms

$P_{K^+}^{int}$	internal partition function for potassium ions
$\bar{Q}_{eA}$	weighted variable cross section for elastic scattering of electrons by argon atoms
$\bar{Q}_{ei}$	weighted variable cross section for elastic scattering of electrons by ions
$\bar{Q}_{eK}$	weighted variable cross section for elastic scattering of electrons by potassium atoms
$\bar{Q}_{es}$	weighted variable cross section for elastic scattering of electrons by s species
Q_{rad}	radiant energy loss
R	radius
$\bar{R}$	universal gas constant
T_e	electron temperature
T_o	gas temperature
$\vec{U}$	velocity
V	potential difference between the two test probes
V_{1A}	first ionization potential of argon
V_{1K}	first ionization potential of potassium
γ	natural line width
γ_p	total line width
δ	energy loss parameter
ε_o	permittivity of free space
η	resistivity
η_o	atomic gas resistivity
η_{ei}	ionic gas resistivity
λ	wavelength of doublet
Λ	parameter defined by Equation (7)

$\Delta\nu^{j}_{c(K-A)}$ half-width due to potassium-argon collisions

$\Delta\nu^{j}_{c(K-K)}$ half-width due to potassium-potassium collisions

$\Delta\nu^{j}_{NAT}$ half-width for natural broadening

ρ function defined by Equation (15)

σ electrical conductivity

$\bar{\sigma}$ standard deviation

$\sigma^{j}_{c(K-A)}$ optical cross section for collisional broadening between the radiating potassium atom and the neutral argon atoms for the $j \rightarrow o$ transition

$\sigma^{j}_{c(K-K)}$ optical cross section for collisional broadening between the radiating potassium atom and the neutral potassium atoms for the $j \rightarrow o$ transition

σ_{ms} diffusion cross section

SUMMARY

The electrical conductivity of an argon-potassium plasma has been experimentally determined as a function of current density for gas temperatures of 1500-1800°K, gas pressures of 15" Hg. Vac. - atmospheric and potassium seeding fractions of 0.002-0.004. Electrical conductivities were measured using two different methods. The first was a continuous method in which the voltage-current response of the plasma to a slowly changing applied voltage was recorded on a strip chart recorder. The second was a pulse technique in which the transient voltage-current response of the plasma to a constant step voltage input was recorded on an oscilloscope.

The electrical conductivity theory of Shelton and Carlson (16) was modified to include the effects of argon ionization and radiation loss from the plasma. The experimental data show good agreement with the modified theory and provide electrical conductivity data for higher current densities (~ 180 amps/cm) than previously available. The effects of gas pressure and potassium seeding fraction predicted by the theory are verified.

The significant peak in electrical conductivity which occurs in the theory of Shelton and Carlson (16) due to the Ramsauer effect of argon tends to become more of a plateau or constant electrical conductivity region in the modified theory because of the importance of argon ionization. The experimental data verify the existence of such a plateau in the electrical conductivity. The modified theory does still predict

a peak in electrical conductivity for some test conditions.

CHAPTER I

INTRODUCTION

Problem Formulation

In the field of magnetohydrodynamic (MHD) power generation, one of the greatest problems is the attainment of high electrical conductivities at gas temperatures which are possible with the materials available today. One method of increasing the electrical conductivity of a gas beyond its equilibrium value uses the nonequilibrium ionization effect. In the reference frame moving with the gas through an MHD generator, there exists an electric field $\vec{E} = \vec{E}^* + \vec{U} \times \vec{B}$ which feeds energy preferentially to the electron gas. This elevated electron energy leads to additional ionization which increases the electrical conductivity of the gas.

Considerable theoretical and experimental work has been done on the nonequilibrium electrical conductivity of alkali-vapor-seeded noble gas plasmas; however, the experimental data has been limited to rather low current densities ($j \leq 80$ amps/cm^2). The data available has been for atmospheric pressure or very low pressure discharges with no data for intermediate pressures. Recent detailed calculations of the nonequilibrium electrical conductivity of an argon-potassium plasma including the energy dependence of the electron-atom collision cross sections (16) indicated that the electrical conductivity reaches a maximum as a function of the current density.

The present investigation was undertaken to obtain nonequilibrium

electrical conductivity data for current densities higher than any previously investigated for comparison with recent theoretical calculations of electrical conductivity. Of special interest was the indicated peak in electrical conductivity predicted by the Shelton and Carlson theory. The effect of gas pressure on the electrical conductivity was also included for intermediate pressures not previously covered in experiments. Modifications to the nonequilibrium electrical conductivity theory were made by including argon ionization and radiant energy losses from the plasma. The experimental results showed good agreement with the modified theory.

Scientific Background

Nonequilibrium ionization due to electron heating has received considerable attention in recent years. The possibility of favorably using this nonequilibrium ionization effect in dense, alkali-vapor-seeded, noble gas plasmas was a result of the work of Kerrebrock and others (1-4).

Kerrebrock (1) developed a simple theory of nonequilibrium electrical conductivity with the assumption of ionization equilibrium at the electron temperature. His two temperature plasma model predicts an electrical conductivity which is a function of the local value of the current density. Kerrebrock obtained measurements of the electrical conductivity in an argon-potassium plasma flowing between two parallel-plate electrodes, perpendicular to the gas flow direction. DC storage batteries supplied the electric field which was used to heat the electrons. Argon gas was bubbled through a pot of molten potassium to obtain the desired

seeding fraction. The experiments were performed at atmospheric pressure with gas temperatures between 1500°K and 2500°K. Current densities in these experiments were limited to less than 30 amps/cm.^{2} Although Joule heating of the neutral gas and electrode sheath effects were neglected, agreement between theory and experiment was achieved by choosing the electron-atom collision cross section and the energy-loss parameter δ for a best fit.

Robben (2) studied the nonequilibrium ionization of an argon-potassium plasma flowing through a segmented electrode MHD generator at a slightly supersonic speed with applied electric and magnetic fields. In all these experiments the gas was at 1500°K and atmospheric pressure. The results of the tests made with an applied electric field agreed with the two temperature model of Kerrebrock after an adjustment of the energy-loss parameter δ. The test made with an applied magnetic field was inconclusive.

Westendorp, et al. (3) and BenDaniel and Bishop (4) studied nonequilibrium ionization in transient discharges in static helium-cesium gases at pressures of 0.1 and 0.2 atmospheres and gas temperatures of 400-500°K. The discharge was produced by the discharge of a capacitor and the electric field within the discharge was measured by two voltage probes inserted in the gas between the electrodes to eliminate electrode sheath effects. The results of these experiments are in general agreement with the ionization predicted by the Saha equation evaluated at the electron temperature. Two different discharge modes were observed, one of which was constricted and the other of which appeared diffuse. The constricted mode was observed only when the cesium density was low or

the current density was large (possibly corresponding to the case when all cesium atoms were ionized). The constriction was delayed by a few hundred microseconds after the application of the test voltage and was accompanied by a marked drop in the voltage difference between the two probes.

Hurwitz, Sutton and Tamor (5) have theoretically analyzed electron heating due to the induced electric field in three different idealized direct current MHD generator geometries. The calculated electrical conductivities and power densities of an argon-potassium plasma in a segmented electrode geometry were higher by one to two orders of magnitude than those achieved in MHD generators using combustion gases at much higher temperatures. Kerrebrock (6) has written a review article which summarizes the present understanding of nonequilibrium ionization as applied to MHD power generation.

In Reference (7), Kerrebrock further developed his proposed two temperature conduction law, giving the range of validity of the proposed law and considering some of its implications. The two temperature model postulates an electron gas composed of the free electrons strongly coupled to the valence electrons of the gas and Maxwellized at its own mean thermal energy. Ionization is assumed to be in equilibrium at the electron temperature. The two temperature conduction law differs from the usual Ohm's law in that the current density is proportional to about the fifth power of the electric field for a slightly ionized gas with an elevated electron temperature. Theoretical calculations (7) based on Kerrebrock's two temperature model, using constant electron-atom collision cross sections and neglecting the radiant energy losses, result in an electrical

conductivity which is a continuously increasing function of the current density. These results lead to questions concerning the current stability of devices using nonequilibrium ionization.

Kerrebrock and Hoffman (8) studied an argon-potassium plasma at atmospheric pressure and gas temperatures of 1400-2000°K. A temperature controlled potassium boiler supplied potassium vapor through a small diameter choked orifice to seed the argon gas. DC storage batteries supplied the voltage for the discharge between two axially placed electrodes. The electric field within the discharge was measured by voltage probes located between the electrodes to eliminate electrode sheath effects. Electrical conductivity measurements covered a range of current densities up to 10 amps/cm^2. Good agreement with Kerrebrock's model was obtained by adjusting the energy loss parameter, δ, in the theory. Radiant energy losses were neglected in this work of Kerrebrock.

Goldstein, et al. (9) have measured the electrical conductivity of a NaK-seeded argon plasma in a Faraday accelerator for $M \approx 1.1$ at atmospheric pressure. Their measurements are in agreement with Kerrebrock's two temperature model for current densities up to 33 amps/cm^2 which was the upper limit of the measurements.

Halstead and Larson (10), experimenting with an argon-potassium plasma, recognized that variable electron-atom collision cross sections could materially affect their results. They neglected electron-ion collisions and applied a correction factor to the values of electrical conductivity predicted by Kerrebrock's theory (1) to account for variable electron-atom cross sections. Average values of the electron-atom cross sections from Brown (11) were used in this correction. The corrected

electrical conductivities gave better agreement with the experimental results; however, current densities were limited to less than 10 amps/cm^2 and radiation energy losses were neglected.

Sheidlin, et al. (12) made electrical conductivity measurements in an argon-potassium plasma at about 1750°K and atmospheric pressure. The gas was heated by an arcjet heater and a potassium boiler was used for seeding the plasma. The results agreed in general with Kerrebrock's earlier work.

Zukoski, et al. (13) made measurements of the nonequilibrium electrical conductivity of an argon-potassium plasma at 2000°K and atmospheric pressure. The plasma flowed through a circular duct with electrodes arranged to give an axial current. Voltage probes were used to measure the electric field between the electrodes. The argon gas was heated with an arcjet heater and potassium seeding was achieved with a potassium boiler. A voltage pulse technique was used to get the voltage-current characteristic of the test section. Measurements of the conductivity were made during the transient period to obtain information about the relaxation phenomena occurring in the plasma in response to a step function change in the applied electric field. It was found that during the first few microseconds, the electrons absorb most of the input power and reach an elevated temperature. Later, the ionization process dominates and is the chief energy sink. After an initial transient period of about 200 microseconds, the temperature of the whole gas system starts to increase due to Joule heating.

Steady-state conductivites were measured for currrent densities from 0.8 to about 90 amps/cm^2. Theoretical calculations were made of

the electrical conductivity of a two temperature plasma including the energy dependence of cross sections and radiation losses from the plasma. The results indicated that radiation losses were small compared to elastic-collision losses when current densities were above 4 amps/cm^2 for the 1/2 in. diameter test section. It was also concluded that for these experiments the conductivity could be closely approximated by using energy-independent cross sections of a properly chosen magnitude. Later measurements by Zukoski and Cool (14) and Cool and Zukoski (15) on essentially the same experimental apparatus gave similar results.

Shelton and Carlson (16) have recently made more detailed calculations of the electrical conductivity of an argon-potassium plasma including the energy dependence of the electron-atom collision cross sections. Ionization of argon atoms was neglected in these calculations. These calculations indicate that the electrical conductivity reaches a maximum as a function of the current density for the argon-potassium plasma. The behavior results theoretically from the pronounced Ramsauer effect of argon. The existence of such a peak in the conductivity indicates current stability.

Bernard, et al. (17) have made calculations of the electrical conductivity for an argon-cesium plasma including variable collision cross sections. A leveling off in the electrical conductivity curve was obtained as the potassium became completely ionized; however, the conductivity then increased again due to argon ionization. Some experimental evidence that such a leveling off in the conductivity actually occurs is presented in Reference (17).

CHAPTER II

ANALYTICAL STUDIES

Electrical Conductivity Theory

The electrical conductivity theory presented here is similar to the calculation of Shelton and Carlson (16) modified to account for the ionization of the argon atoms and the radiant energy loss from the plasma. An expression for the electrical conductivity is obtained by taking the momentum moment of Boltzmann's equation and evaluating the collision term by using Morse's collision integrals (18):

$$\frac{1}{\sigma} = \eta = \frac{4}{3}\left(\frac{8kT_e}{\pi m_e}\right)^{\frac{1}{2}} \frac{m_e}{n_e e^2} \sum_s n_s \bar{Q}_{es} \tag{1}$$

where, σ = electrical conductivity

η = electrical resistivity

$\bar{Q}_{es}$ = weighted variable cross section for elastic scattering of electrons by the s species.

The weighted variable cross section for elastic scattering of electrons by the s species is defined by the following expression:

$$\bar{Q}_{es} \equiv \left(\frac{m_e}{2kT_e}\right)^3 \int_o^\infty \exp\left(-\frac{m_e g^2}{2kT_e}\right) \sigma_{ms} g^5 dg \tag{2}$$

where, σ_{ms} = diffusion cross section.

For the particular case of an argon-potassium plasma, Equation (1) becomes:

$$\eta = \frac{4}{3}\left(\frac{8kT_e}{\pi m_e}\right)^{\frac{1}{2}} \frac{m_e}{n_e e^2} \left(n_A \bar{Q}_{eA} + n_K \bar{Q}_{eK} + n_i \bar{Q}_{ei}\right) \tag{3}$$

Equation (3) can be separated into two parts as follows:

$$\eta = \eta_o + \eta_{ei} \tag{4}$$

$$\eta_o = \frac{4}{3}\left(\frac{8kT_e}{\pi m_e}\right)^{\frac{1}{2}} \frac{m_e}{n_e e^2}\left(n_A \bar{Q}_{eA} + n_K \bar{Q}_{eK}\right) \tag{5}$$

$$\eta_{ei} = \frac{4}{3}\left(\frac{8kT_e}{\pi m_e}\right)^{\frac{1}{2}} \frac{m_e}{n_e e^2}\left(n_i \bar{Q}_{ei}\right) \tag{6}$$

where, η_o = atomic gas resistivity

η_{ei} = ionic gas resistivity.

Notice that Equation (4) is a result of the electrical conductivity calculational method and not the assumption of Lin, Resler and Kantrowitz (19).

Spitzer and Härm (20) give an expression for the ionic gas resistivity which was used in Reference (16) to replace Equation (6):

$$\eta_{ei} = \frac{6.53 \times 10^3}{T_e^{3/2}} \ln \Lambda \tag{7}$$

where,

$$\Lambda = \frac{12\pi}{e^3 n_e^{1/2}} (\varepsilon_o k T_e)^{3/2}$$

The Spitzer-Härm resistivity includes the effects of electron-electron interactions on the distribution function.

The expression for electron energy is obtained by taking the energy moment of Boltzmann's equation and using Morse's collision integrals:

$$\frac{j^2}{\sigma} = 4 n_e k \left(\frac{8kT_e}{\pi m_e}\right)^{\frac{1}{2}} (T_e - T_o) \frac{m_e}{m_A} \sum_s n_s \bar{Q}_{es} + Q_{rad} \qquad (8)$$

where, T_e = electron temperature

T_o = gas temperature

$\bar{Q}_{rad}$ = radiant energy loss

By making use of Equation (1) for the electrical conductivity, Equation (8) becomes:

$$j^2 = \frac{3 n_e^2 e^2 k}{2 m_A} (T_e - T_o) + \sigma Q_{rad} \qquad (9)$$

An expression for the radiant energy loss from the plasma is presented in the next section.

Considering ionization of both potassium and argon atoms, the electron density is obtained from the following two Saha equations assuming ionization equilibrium at the electron temperature:

$$\frac{n_e n_A^+}{n_A} = E_A = \frac{p_e^{int} p_{A^+}^{int}}{p_A^{int}} \left(\frac{2\pi m_e kT_e}{h^2}\right)^{\frac{3}{2}} \exp\left(-\frac{V_{1A} e}{kT_e}\right) \qquad (10)$$

where, V_{1A} = first ionization potential of argon

n_A = number density of argon atoms

n_A^+ = number density of argon ions

p_e^{int} = internal partition function for electrons

$p_{A^+}^{int}$ = internal partition function for argon ions

p_A^{int} = internal partition function for argon atoms

and,

$$\frac{n_e n_K^+}{n_K} = E_K = \frac{p_e^{int} p_{K^+}^{int}}{p_K^{int}} \left(\frac{2\pi m_e kT_e}{h^2}\right)^{\frac{3}{2}} \exp\left(-\frac{V_{1K} e}{kT_e}\right) \qquad (11)$$

where, V_{1K} = first ionization potential of potassium

n_K = number density of potassium atoms

n_K^+ = number density of potassium ions

p_e^{int} = internal partition function for electrons

$p_{K^+}^{int}$ = internal partition function for potassium ions

p_K^{int} = internal partition function for potassium atoms.

The additional condition of charge neutrality is necessary to supply the following equation:

$$n_e = n_A^+ + n_K^+ \tag{12}$$

Using Dalton's law of partial pressures and the assumption that the electron pressure is negligible, the following equation is obtained:

$$P = (n_A + n_A^+ + n_K + n_K^+)kT_o \tag{13}$$

By definition, the seeding fraction is represented by:

$$F \equiv \frac{n_K + n_K^+}{n_A + n_A^+} \tag{14}$$

By combining Equations (10), (11), (12), (13) and (14), an equation for the electron density is obtained.

$$n_e^2 + E_K n_e - \frac{PF}{(1 + F)kT_o}(1 + \rho)E_K = 0 \tag{15}$$

where, $$\rho = \frac{E_A}{FE_K}\frac{E_K + n_e}{E_A + n_e} = \frac{n_A^+}{n_K^+}$$

By using Equations (10), (11), (12), (13) and (14), Equation (4) can be put into the following form:

$$\frac{1}{\sigma} = \eta = \frac{4}{3}\left(\frac{8kT_e}{\pi m_e}\right)^{\frac{1}{2}} \frac{m_e}{e^2} \frac{P}{(1 + F)kT_o}\left[\frac{\bar{Q}_{eA}}{n_e + E_A} + \frac{F\bar{Q}_{eK}}{n_e + E_K}\right] \tag{16}$$

$$+ \frac{6.53 \times 10^3}{T_e^{3/2}} \ln\left[\frac{12\pi}{e^3 n_e^{1/2}}(\varepsilon_o kT_e)^{3/2}\right]$$

The set of equations (9), (15) and (16) along with the radiant energy loss term from the next section were solved for an argon-potassium plasma on a Burroughs 5500 computer using the values of $\bar{Q}_{eA}$ and $\bar{Q}_{eK}$ from Kruger and Viegas (21) for $1000^{\circ}K \leq T_e \leq 10{,}000^{\circ}K$. The energy dependence of the weighted cross sections $\bar{Q}_{eA}$ and $\bar{Q}_{eK}$ is illustrated in Figure (1). The very small cross section for argon at an electron temperature of about $1800^{\circ}K$ is known as the Ramsauer effect and is present in the cross section data for most noble gases.

The modified theory is compared with the Shelton and Carlson theory (16) in Figure (2) for a gas temperature of $1500^{\circ}K$, a gas pressure of 15" Hg. vacuum and a seeding fraction of 0.002. The ionization of argon atoms is seen to significantly change the theoretical curve for current densities above about 80 amps/cm^2 which corresponds to an electron temperature of about $8000^{\circ}K$. For most test conditions, the peak in the electrical conductivity curve predicted by the unmodified theory is reduced to a plateau region of constant electrical conductivity after which the conductivity increases once again due to the argon ionization. There are, however, run conditions for which the modified theory does predict a slight peak in electrical conductivity. All of the terminal points of the theoretical curves shown correspond to an electron temperature of $10{,}000^{\circ}K$, thus the modified theory predicts a much slower increase in the electron temperature with current density than the unmodified theory after the start of argon ionization. This variation in electron temperature is shown in Figure (3). An explanation of these curves is obtained from the electron energy equation, Equation (9), which can be rearranged in the following form:

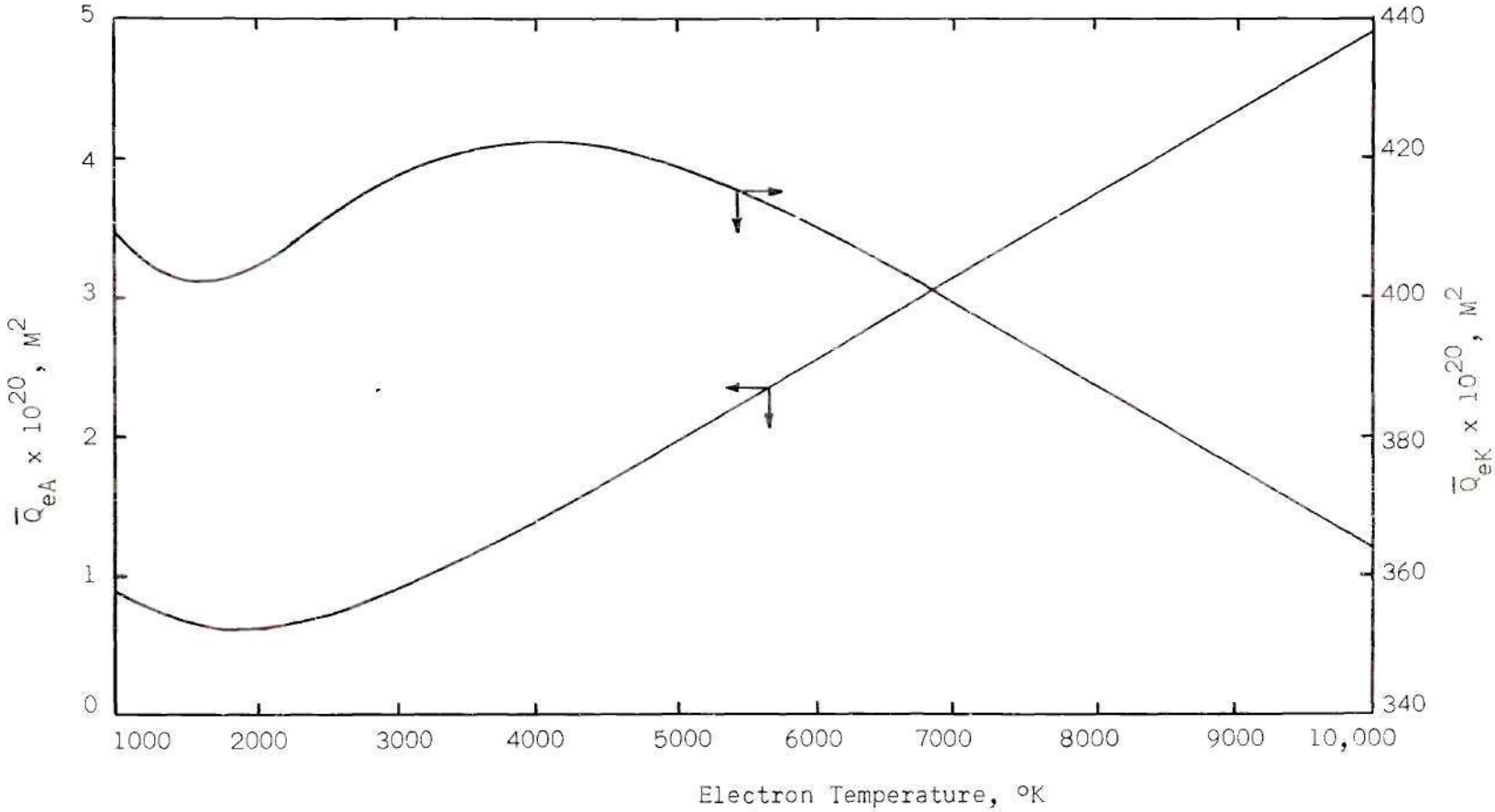

Figure 1. Energy Dependence of Weighted Cross Section $\bar{Q}_{eA}$ and $\bar{Q}_{eK}$.

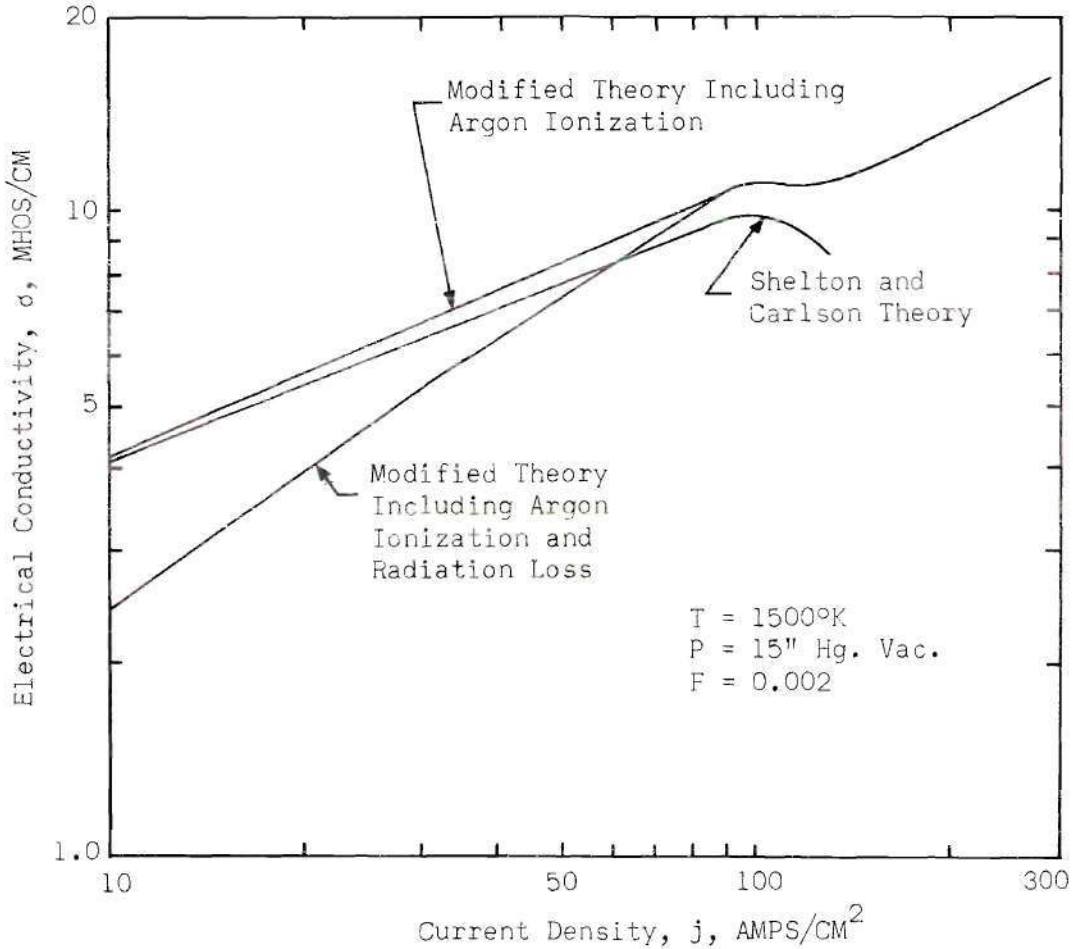

Figure 2. Comparison of Electrical Conductivity Theories.

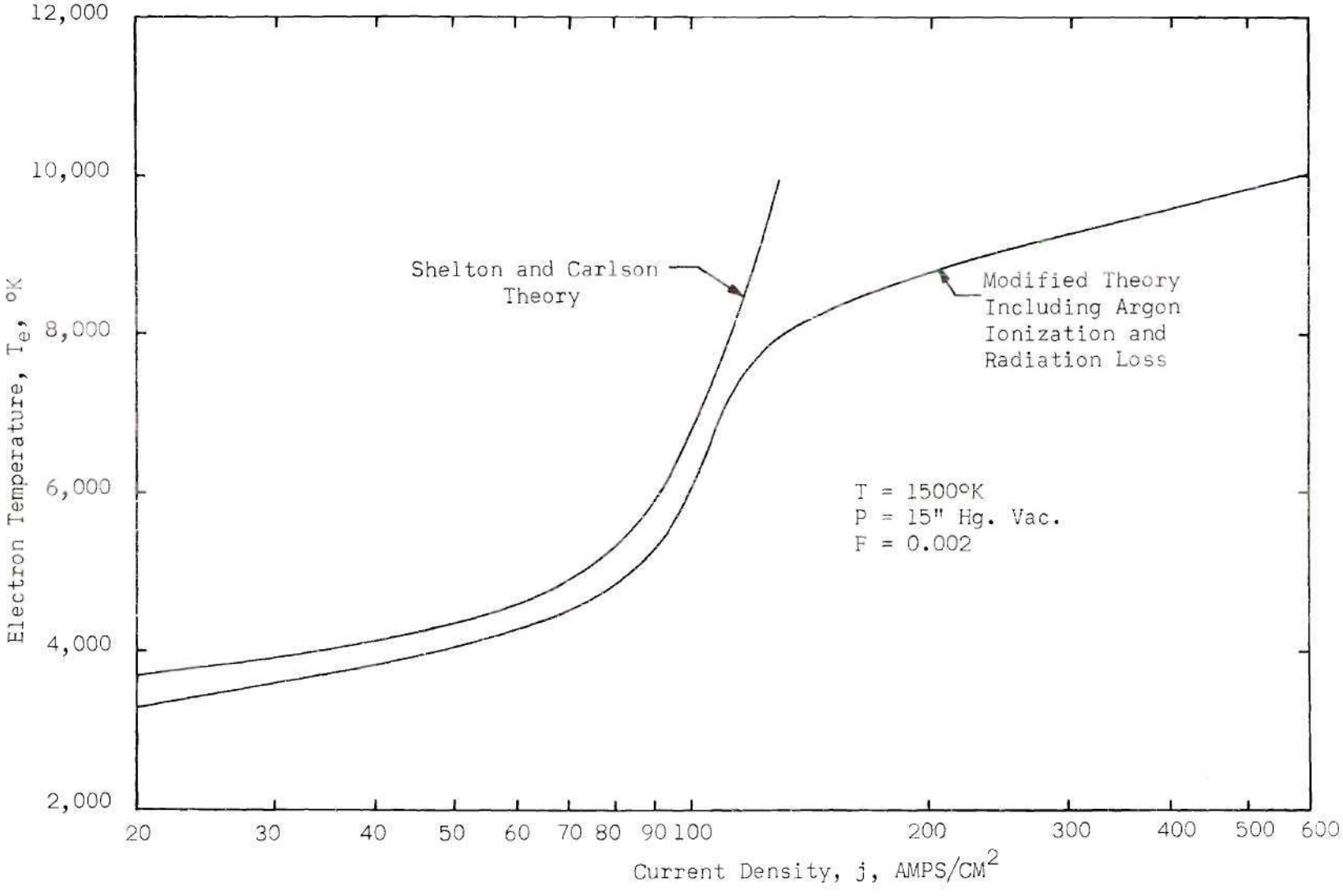

Figure 3. Electron Temperature Versus Current Density.

$$T_e = T_o - \frac{2m_A}{3e^2k}\left(\frac{\sigma Q_{rad}}{n_e^2}\right) + \frac{2m_A}{3e^2k}\left(\frac{j^2}{n_e^2}\right) \qquad (9')$$

The second term on the right hand side (RHS) of Equation (9') is due to the radiant energy loss from the plasma. This radiant energy is an energy loss from the electron gas, which results in a lower electron temperature than that predicted by the unmodified theory. Consider the effect of the third term on the RHS of Equation (9') for systems with different current densities and the same gas temperatures, gas pressures and seeding fractions. For systems with low current densities, a larger j is accompanied by a larger n_e due to potassium ionization, which results in little change in T_e. For systems with intermediate current densities, a larger j is accompanied by little change in n_e since most of the potassium atoms are ionized and the electrons have insufficient energy to ionize the argon atoms. This results in a larger T_e for the systems with larger j. For systems with large current densities, a larger j is accompanied by a larger n_e due to argon ionization, which results in little change in T_e.

The radiant energy loss calculations were made for the particular experimental apparatus used in these tests and is therefore valid only for comparing the results of these tests with the theory. For low current densities, radiation losses become comparable to the elastic collision losses and result in lower values of the electrical conductivity.

Radiant Energy Loss

The importance of the consideration of radiant energy loss from the plasma in comparing experimental data with the two temperature

electrical conductivity model has been shown by Zukoski, Cool, and Gibson (13), who obtained much better agreement with theory after correcting the theory for radiant energy loss.

Lutz (22) has made a detailed calculation of the radiant energy loss from a cesium-argon plasma between two infinite parallel plates. He shows that the principal part of the radiant energy loss is due to the resonance lines for electron temperatures below 3000°K.

In general, the radiation loss is given by

$$Q_{rad} = \sum_{j} G_j h\nu_j n_j A_{j\to o} \tag{17}$$

where, G_j = resonance escape factor

$A_{j\to o}$ = Einstein spontaneous emission probability

$h\nu_j$ = energy of transition from the j^{th} level to the ground state

n_j = number density of the j^{th} state.

According to Lutz (22), the effects of Stark and Doppler broadening of the spectral lines is negligible in comparison with collisional broadening. For the case of collisional broadening Holstein (23) gives the following formula for the resonance escape factor for an infinite cylinder of radius R.

$$G_j = 1.115 \left[\frac{2g_o \nu_j^2}{c^2 n_o g_j R} \left(\frac{\gamma_p}{\gamma}\right)_j \right]^{\frac{1}{2}} \tag{18}$$

where, R = radius of the cylinder

g_o = statistical weight of the ground state

g_j = statistical weight of the j^{th} excited state

n_o = density of atoms in ground state

γ = natural line width

γ_P = total line width.

Considering collisional broadening due to collisions with argon and potassium atoms, the ratio $(\gamma_P/\gamma)_j$ can be written as:

$$\left(\frac{\gamma_P}{\gamma}\right) = \frac{\Delta\nu^j_{nat} + \Delta\nu^j_{c(K-K)} + \Delta\nu^j_{c(K-A)}}{\Delta\nu^j_{nat}} \tag{19}$$

where, $\Delta\nu^j_{nat}$ = half-width for natural broadening

$\Delta\nu^j_{c(K-K)}$ = half-width due to K-K collisions

$\Delta\nu^j_{c(K-A)}$ = half-width due to K-A collisions

Now, neglect the excitation of argon atoms and consider only the $4P_{1/2} \rightarrow 4S_{1/2}$ and $4P_{3/2} \rightarrow 4S_{1/2}$ transitions in the potassium atoms. Use the correspondence

$$0 \rightarrow 4S_{1/2}$$

$$1 \rightarrow 4P_{1/2}$$

$$2 \rightarrow 4P_{3/2}$$

and consider only these 3 states of potassium to be populated according to a Boltzmann distribution at the electron temperature. Thus,

$$n_K = n_K^o + n_K^1 + n_K^2 \tag{20}$$

where, n_K = number density of neutral potassium atoms

n_K^o = number density of potassium atoms in ground state

n_K^1 = number density of potassium atoms in the $4P_{1/2}$ excited state

n_K^2 = number density of potassium atoms in the $4P_{3/2}$ excited state.

By definition of the Boltzmann distribution

$$\frac{n_K^1}{n_K^o} = \frac{g_1}{g_o} e^{-\frac{h\nu_1}{kT_e}} \quad \text{and} \tag{21}$$

$$\frac{n_K^2}{n_K^o} = \frac{g_2}{g_o} e^{-\frac{h\nu_2}{kT_e}} \tag{22}$$

Combining Equations (20), (21) and (22) get:

$$n_K^o = \frac{n_K}{1 + (\frac{g_1 + g_2}{g_o}) e^{-\frac{h\nu}{kT_e}}} \tag{23}$$

Considering the two excited states of potassium, Equation (17) can be written in the following way by expressing the Einstein spontaneous emission probabilities in terms of the emission oscillator strengths.

$$Q_{rad} = \frac{2\pi e^2 n_K^o h}{m_e \lambda^3 \varepsilon_o g_o}\left[G_1 g_1 f_{1\to o} + G_2 g_2 f_{2\to o}\right] e^{-\frac{h\nu}{kT_e}} \qquad (24)$$

where, λ = wave length of doublet

$f_{1\to o}$ = emission oscillator strength of the $4P_{1/2}$ level

$f_{2\to o}$ = emission oscillator strength of the $4P_{3/2}$ level.

For the present calculation equations (18) and (19) yield the following set of equations:

$$G_j = 1.115\left[\frac{2g_o \nu_j^2}{c^2 n_K^o g_j R}\left(\frac{\gamma_P}{\gamma}\right)_j\right]^{\frac{1}{2}} \qquad (j = 1,2) \qquad (25)$$

where,

$$\left(\frac{\gamma_P}{\gamma}\right)_j = \frac{\Delta\nu^j_{nat} + \Delta\nu^j_{c(K-K)} + \Delta\nu^j_{c(K-A)}}{\Delta\nu^j_{nat}} \qquad (j = 1,2) \qquad (26)$$

The following equations for half-widths due to collisional broadening are taken from Mitchell and Zemansky (24):

$$\Delta\nu^j_{nat} = \frac{e^2 \nu_j^2}{m_e c^3} f_{j\to o} \qquad (j = 1,2) \qquad (27)$$

$$\Delta\nu^j_{c(K-K)} = \frac{2}{\pi}\left[\sigma^j_{c(K-K)}\right]^2 n_K^o \sqrt{2\pi \bar{R} T_o \left(\frac{1}{\tilde{M}_K} + \frac{1}{\tilde{M}_K}\right)} \qquad (j = 1,2) \qquad (28)$$

$$\Delta\nu^{j}_{c(K-A)} = \frac{2}{\pi}\left[\sigma^{j}_{c(K-A)}\right]^{2} n_A \sqrt{2\pi\bar{R}T_o\left(\frac{1}{\tilde{M}_K}+\frac{1}{\tilde{M}_A}\right)} \qquad (j=1,2) \qquad (29)$$

where, $\sigma^{j}_{c(K-K)}$ = optical cross section for collisional broadening between radiating potassium atom and neutral potassium atoms for the $j \rightarrow 0$ transition

$\sigma^{j}_{c(K-A)}$ = optical cross section for collisional broadening between radiating potassium atoms and neutral argon atoms for the $j \rightarrow 0$ transition.

$\bar{R}$ = universal gas constant

$\tilde{M}_K$ = molecular weight of potassium

$\tilde{M}_A$ = molecular weight of argon.

The calculation of the radiant energy loss reduces to solving the set of Equations (24), (25), (26), (27), (28) and (29). The following constants were used in this calculation:

$f_{1\rightarrow o} = f_{2\rightarrow o} = 0.35$ Kerrebrock (6)

$\lambda_1 = 7664.91$ Å

$\lambda_2 = 7698.98$ Å

$g_o = 2$

$g_1 = 4$

$g_2 = 2$

$$\sigma^1_{c(K-K)} = \sigma^1_{c(K-A)} = 6.04 \times 10^{-19}\ m^2$$

Hofmann and Kohn (25)

$$\sigma^2_{c(K-K)} = \sigma^2_{c(K-A)} = 5.77 \times 10^{-19}\ m^2$$

$R = 0.675$ cm.

CHAPTER III

EXPERIMENTAL STUDIES

Experimental Facilities

The experimental facilites used in these experiments can be divided into the following seven major parts: (1) gas supply and arc torch, (2) seeding apparatus, (3) mixing chamber, (4) test section, (5) calorimeter, (6) vacuum system and (7) auxiliary systems and instrumentation. These major divisions are shown in Figure (4). Each of these parts will be discussed separately so that changes and modifications leading to the final system can be discussed.

The primary argon gas supply consisted of 5 bottles of welding grade argon with impurities of less than 30 ppm fed through a common gas manifold. The gas pressure of the argon gas leaving the manifold was controlled by a 0-1500 psig Airco pressure regulator. A secondary argon gas supply consisting of a single bottle of welding grade argon controlled by a 0-300 psig National pressure regulator was provided for use with the seeding apparatus.

The primary argon gas was heated by a Thermal Dynamics Model F-80 Thermal Arc Torch with DC electrical power supplied by a Miller Selenium Rectifier Model 1500 C-1 with a rated capacity of 83.2 kilowatts. The rectifier can supply 40, 80 or 160 volts open circuit voltage on the secondary side for use by the torch. For the majority of the tests, the rectifier open circuit voltage was set at 160 volts.

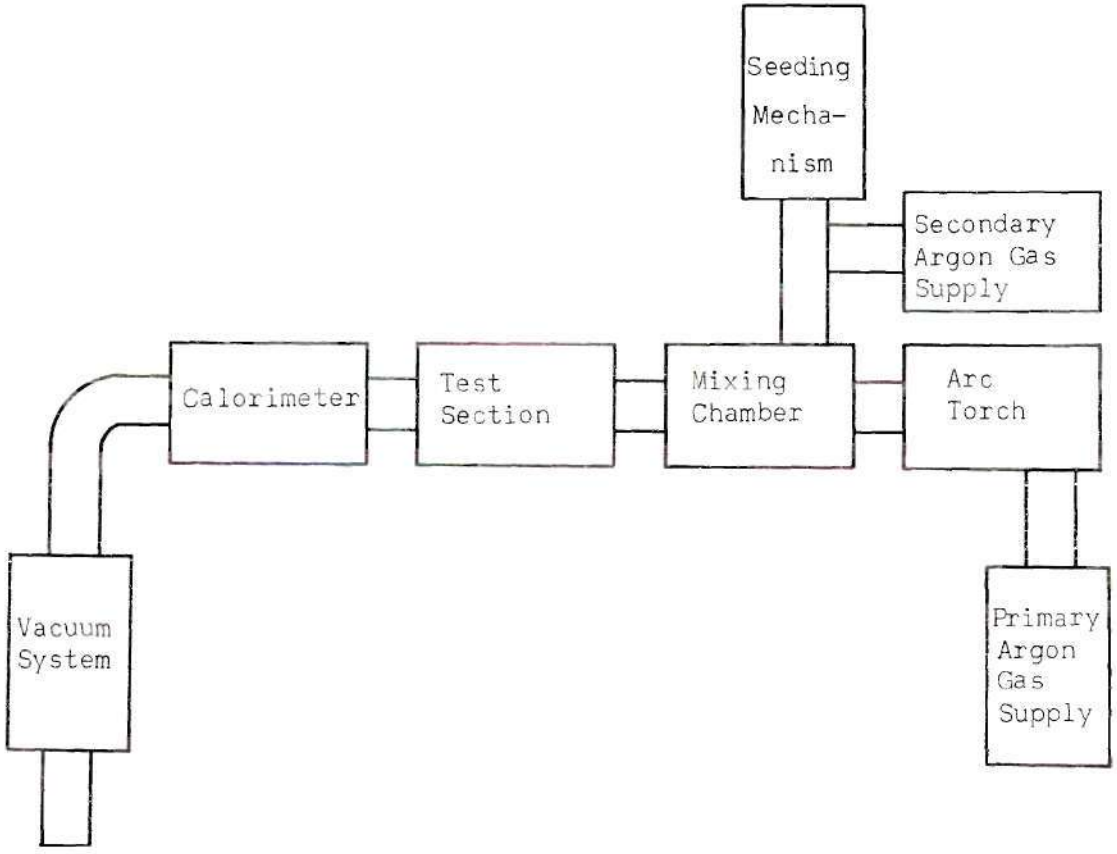

Figure 4. Experimental Facilities.

Control of the operation of the torch was provided by a Thermal Dynamics Thermal Arc Automatic Control Console Model 50 NHB. The primary argon gas and the cooling water for the arc torch pass through the control console before going to the arc torch. The primary argon gas is regulated and metered in the control console. The control console has several safety interlocks built in to protect the torch from damage. If the torch cooling water pressure drops below 90 psig or if the primary argon gas supply is lost, the torch is automatically stopped. The control console contains the start, ignite and stop buttons as well as the amperage control for the arc torch.

The seeding apparatus for the seeding of the argon gas with potassium was a positive displacement device driven by a variable speed motor. Two different designs were tried and both will be described. Design A is shown in Figure (5). Design A consisted of a stainless steel potassium container having a 0.020" diameter opening in the bottom for feeding potassium into the gas system. The secondary argon gas stream was heated to about 400°C by a nichrome wire heating element and passed by the small opening to help break up the liquid drops of potassium being pushed out of the potassium container. A 1/4 inch inside diameter stainless steel cylinder and piston was located above the potassium container. Kerosene was used to cover the potassium and fill the feed cylinder. The use of kerosene in contact with the movable piston permitted the use of a rubber o-ring seal on the piston. The piston was displaced by a screw mechanism driven by an electric motor controlled by a Heathkit Model GD-973A Motor Speed Controller. The temperature of the potassium container was maintained at about 170°C by a nichrome heating element to keep the potassium

in the liquid state. This seeding apparatus was not adapted to start and stop operation. If the test was made immediately after loading the potassium, successful seeding was possible. Attempts to use the same potassium loading for several tests failed because of the potassium shrinkage upon cooling and its adhesion to the walls of the potassium container. These effects resulted in a mixture of kerosene and potassium being obtained from the seeding apparatus when used for the second time.

Design B of the seeding apparatus, which is shown in Figure (6), consisted of a 10cc B-D Luer-Lok Syringe with a one inch long 24 gauge B-D needle, a syringe holder and a variable speed motor dirve for displacing the piston. Before loading the syringe with potassium, a thin coating of Dow Corning silicone high vacuum grease was applied to the piston of the syringe to prevent any leakage of potassium by the piston during a test. After loading the syringe with potassium, the syringe was placed in a copper syringe holder which was pre-heated to about 200°C to prevent solidification of the potassium. The secondary argon gas, heated to about 400°C by nichrome wire heating element, was passed by the needle tip to help break up the potassium drop formation on the needle tip. The piston was displaced by the same variable speed motor screw drive as Design A. Design B was more successful in supplying known quantities of seeding material than Design A. Design B was used for the majority of the tests reported.

The initial mixing section was a water cooled, 1/2 inch diameter stainless steel tube 10 diameters in length. The potassium seed material was injected into the primary argon gas stream as the argon left the arc torch. Thus, the potassium had a distance of 10 diameters in which to

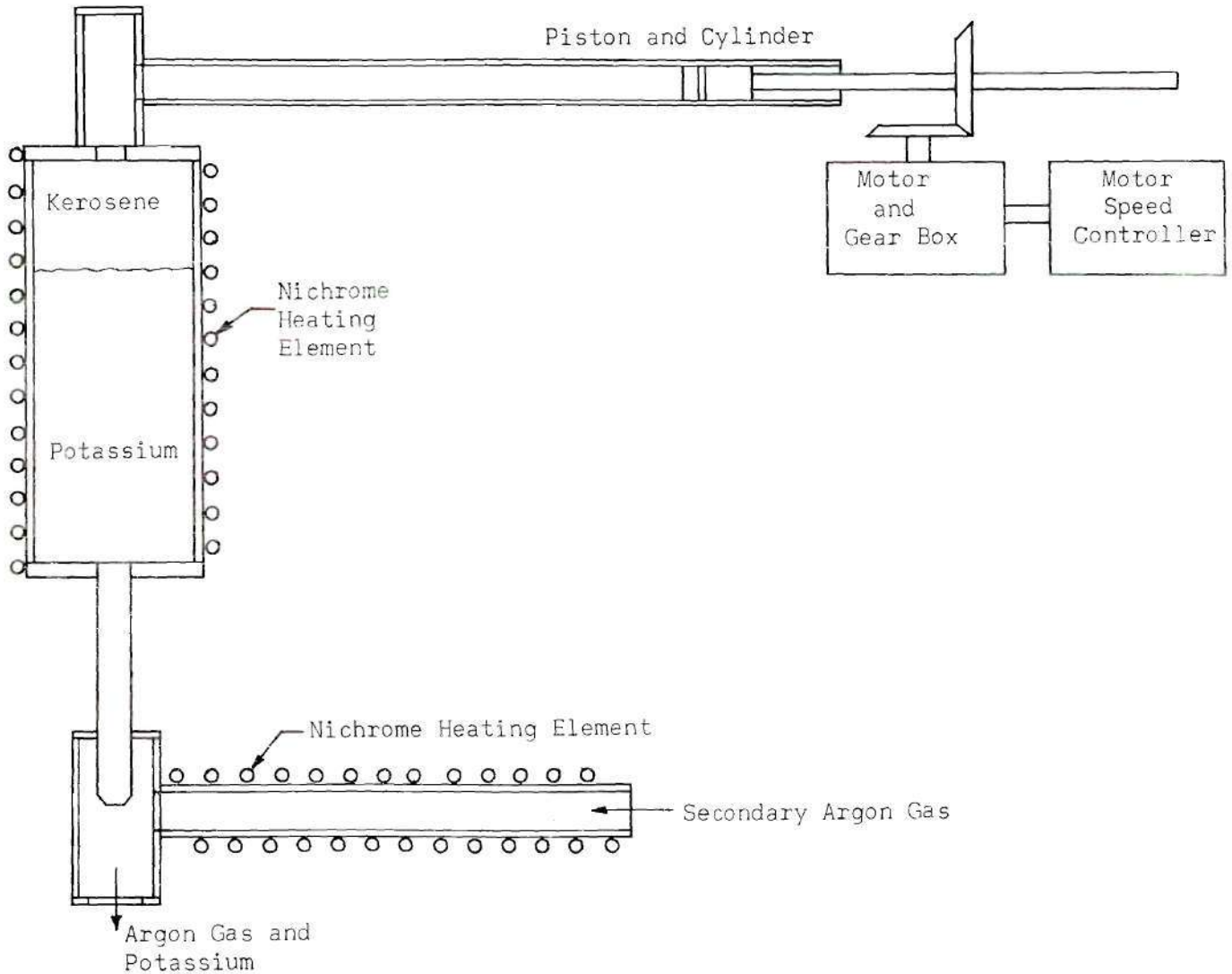

Figure 5. Seeding Mechanism - Design A.

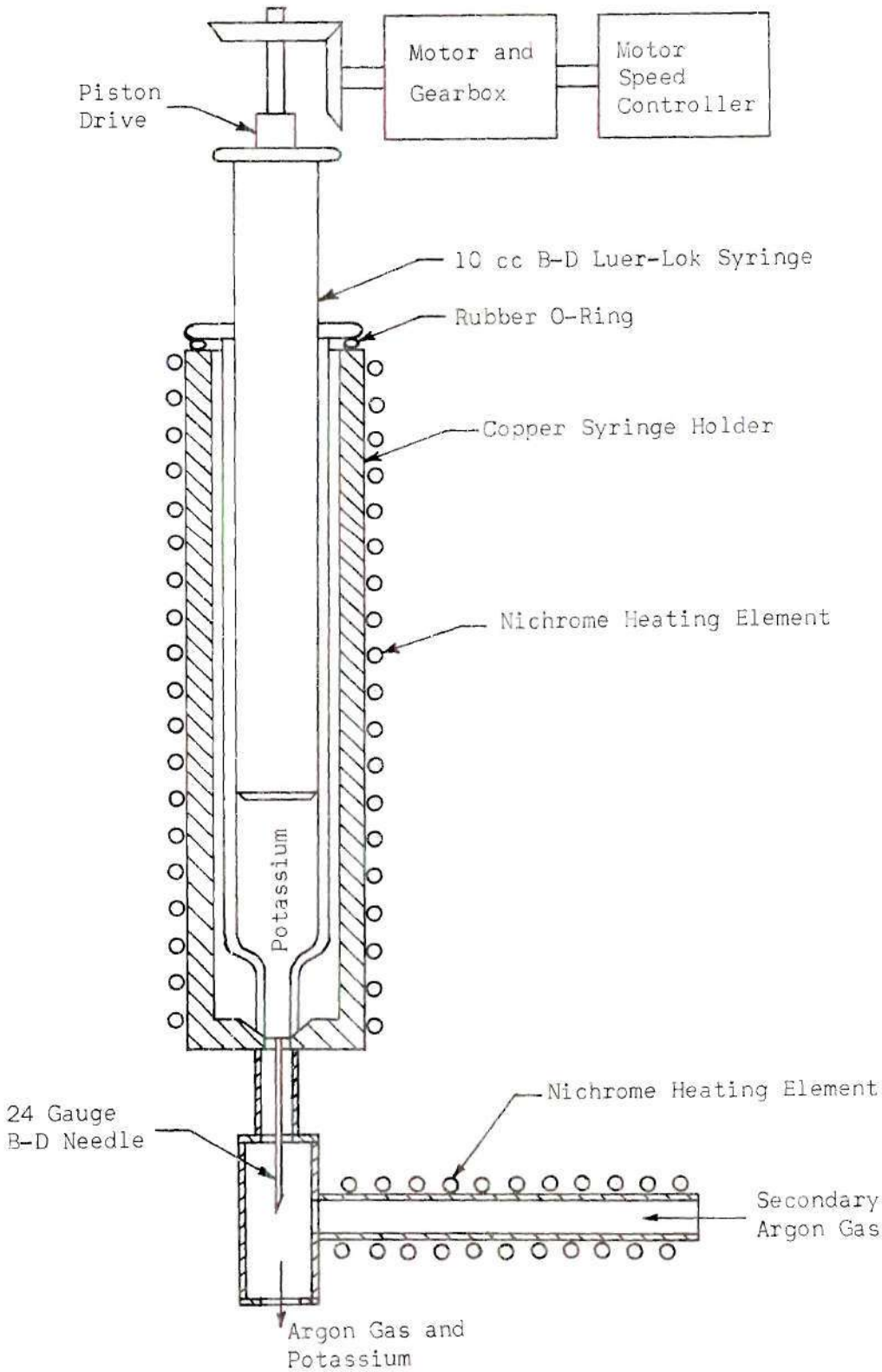

Figure 6. Seeding Mechanism - Design B.

ionize and mix with the primary gas stream before reaching the test section. The purpose of having a cooled mixing section was to enable a heat balance to be made of the gas upstream of the test section to determine the enthalpy of the gas entering the test section. The cooling of the mixing section wall resulted in the condensation of potassium on the cool surfaces causing the seeding to be very erratic and non-uniform. Thus, it was necessary to use an uncooled mixing section.

The second mixing section was an uncooled stainless steel tube with a graphite insert for the hot gases to pass through. This mixing section was not very successful because of the graphite dust which passed through the test section. This graphite, which is an electrical conductor, caused erratic voltage reading from the voltage probes in the test section. The final mixing section design was an air-cooled stainless steel tube with a boron nitride insert having a 1/2 inch diameter gas passage. The boron nitride was 10 diameters in length which allowed time for the mixing of the argon-potassium stream before entering the test section.

The test section consisted of an uncooled stainless steel tube with a boron nitride insert. The test section inside diameter was 1/2 inch with an overall length of 5 inches. Boron nitride was found to be an excellent material for use in the test section because of its electrically insulating and high temperature properties. The test section is shown schematically in Figure (7). The test section electrodes were spaced axially. The upstream electrode or anode was a stainless steel ring electrode, while several different types of downstream electrodes or cathodes were tried. The axial spacing of the electrodes was chosen over a parallel plate arrangement since additional electrode area could be provided for

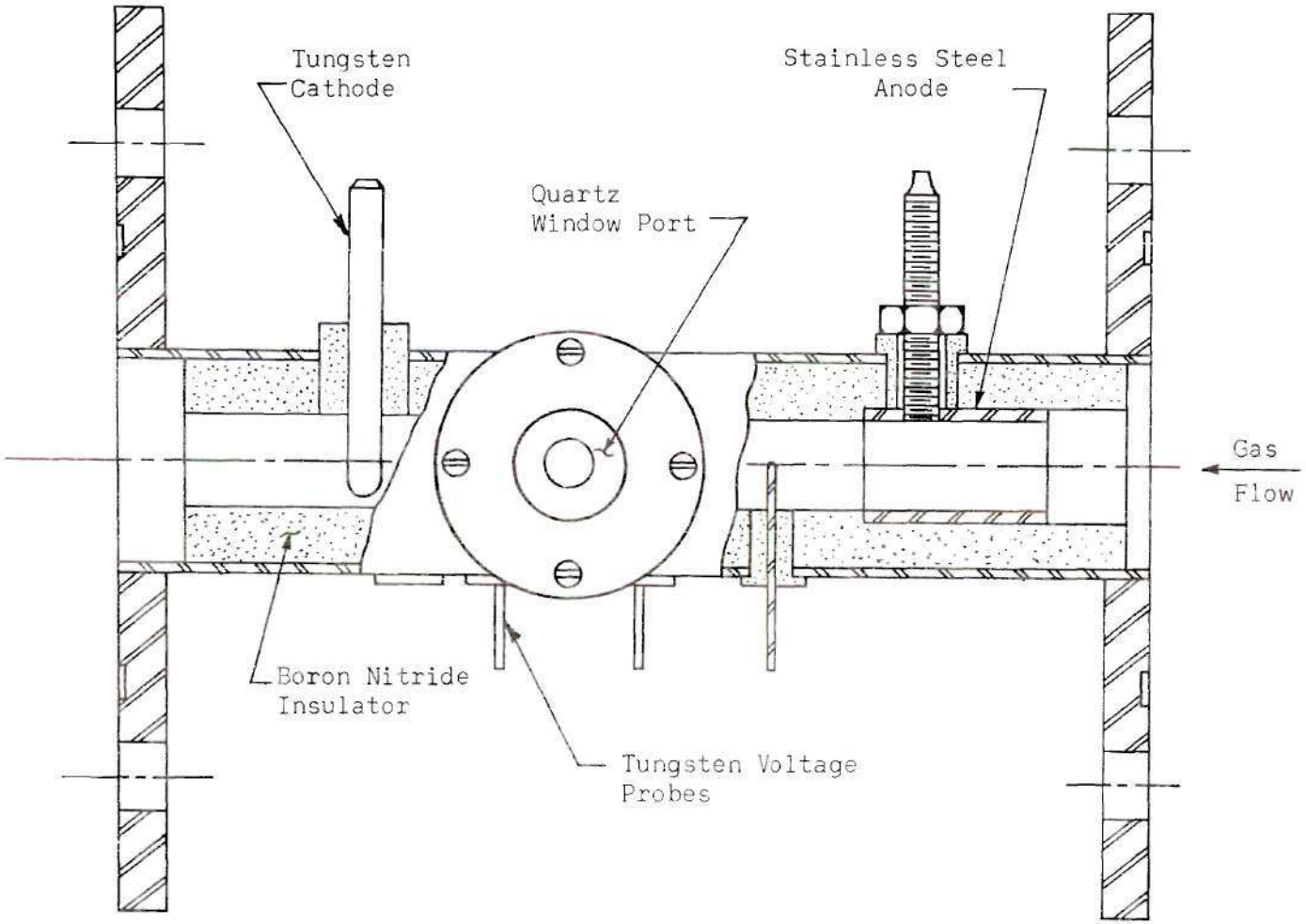

Figure 7. Test Section.

the thermionic emission of the necessary electrons for the high current densities of interest in these experiments. A ring electrode was used for the anode to allow an unobstructed flow of gas through the test section. Both stainless ring electrodes and 3/16 inch diameter tungsten rod electrodes were used as the cathode. The data obtained with the two cathode configurations were very similar; however, the tungsten electrodes lasted much longer and for this reason were the more desirable type.

Tungsten wire voltage probes of 0.060 inch diameter were inserted in the flow between the electrodes as shown in Figure (7). The voltage distribution in the test section was measured with these probes, which allowed the determination of the electric field without the sheath effect errors due to electrode geometry. Several runs showed that the electric field was fairly constant except for a region close to the electrodes; therefore, the remainder of the tests were made with only two voltage probes between the electrodes.

Two quartz window ports were provided between the electrodes for visual observation of the discharge and also for the measurement of the gas temperature with an optical pyrometer.

The calorimeter or heat exchanger was designed to remove energy from the plasma stream so that the gas could pass through the vacuum system without causing damage. The calorimeter is shown in Figure (8). It is constructed entirely from copper and brass material and has three concentric gas passes. All interior gas passages are protected by 1/4 inch O. D. copper cooling coils. Since the calorimeter contains approximately 150 feet of 1/4 inch O.D. cooling water passages, three parallel

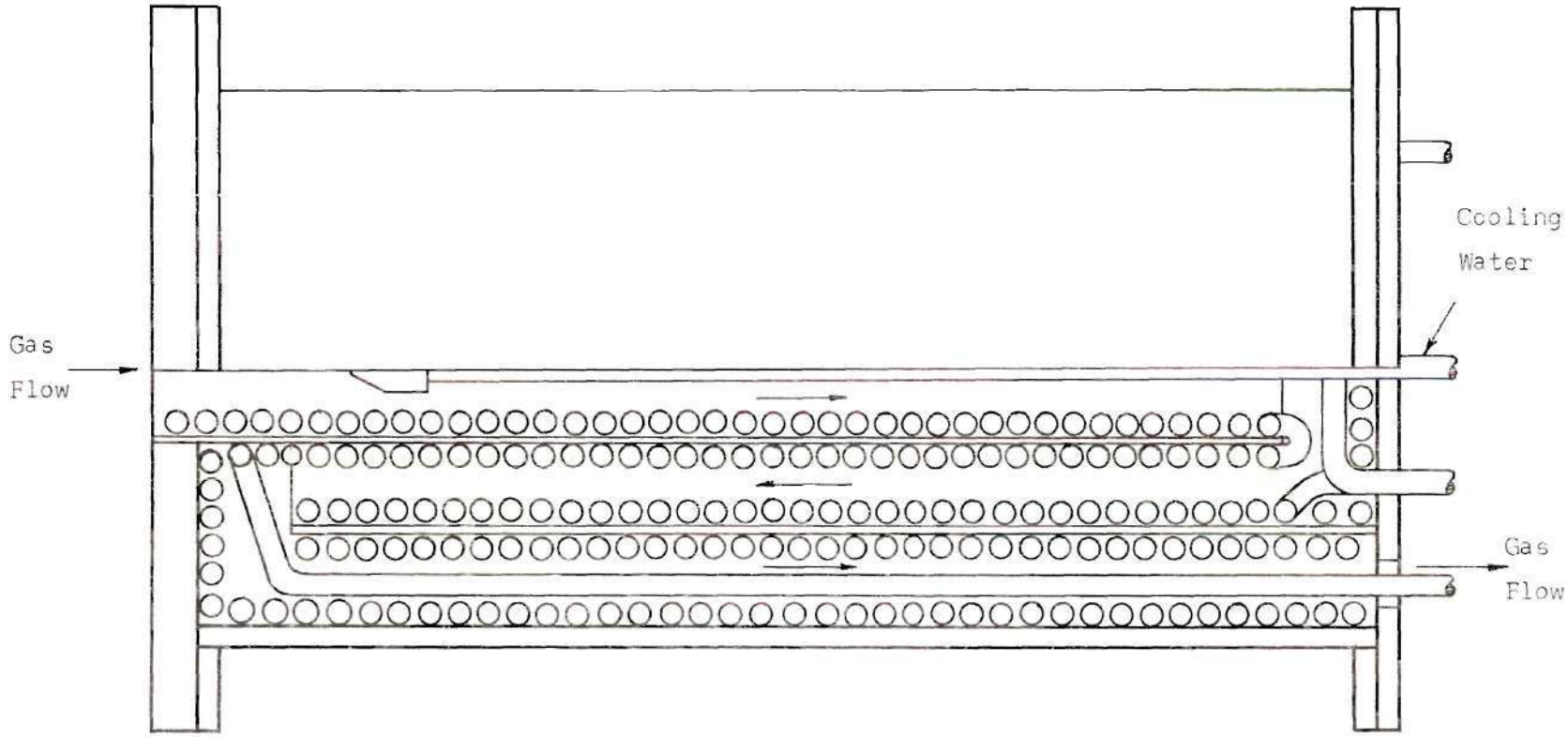

Figure 8. Calorimeter.

cooling water passes of 50 feet each are used to cut down on the cooling water pressure drop. Upon entering the calorimeter, the hot plasma gases strike a cooled diverter body located in the center of the tube. This diverter body helps remove a large portion of the gas energy during the first pass through the calorimeter by increasing the stream turbulence and also increasing the heat transfer area.

The vacuum system consists of a Leiman rotary oil-less pump Model 297-6 with a capacity of 30 cubic feet of argon per minute (under the vacuum condition) at a vacuum of 15 in. Hg. An oil-less pump was specified since trace quantities of potassium could remain in the gas stream upon entering the vacuum pump. As a further precaution against getting potassium in the vacuum system, a gas filter was installed immediately upstream of the vacuum pump. To permit some control over the test section pressure, an air bleed valve was provided between the heat exchanger and the vacuum pump.

The water cooling system provided the cooling capacity for the arc torch and the calorimeter from the standard water supply available in the laboratory. A diagram of the water cooling system is shown in Figure (9). Upon leaving the laboratory water supply line, the water is filtered by passing it through a Fram Model FS 1133-PL water filter. The water pressure is increased to the necessary value by a 3/2-DN4 Worthington Monobloc water pump. The water pump was necessary because of the cooling water capacity and pressure requirements of the arc torch. After passing through the pump, the cooling water goes to the arc torch control console. In the control console the water passes through a solenoid relay which shuts off the arc torch if the cooling water pressure drops below 90 psig. The

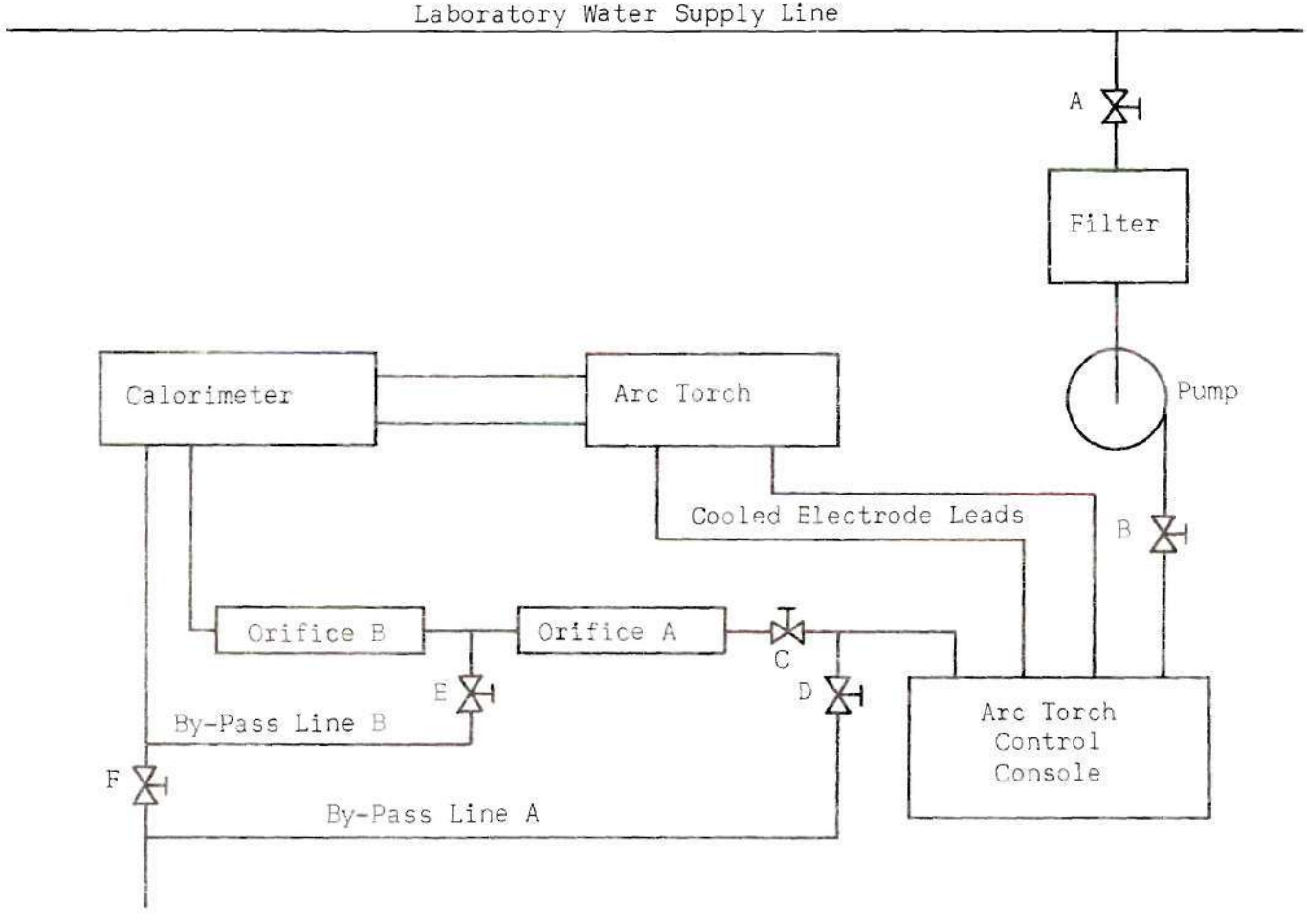

Figure 9. Water Cooling System.

water goes from the control console through the cooled cathode lead to the arc torch and after passing through the cooling passages of the arc torch returns to the control console through the cooled anode lead. The control console is equipped with an air purge system for removing the cooling water from the electrode leads and arc torch when the torch is not in operation. When the air purge is to be used, the cooling water and air pass through by-pass line A upon leaving the control console. When the torch is in operation, the by-pass line A is closed off and all cooling water passes through orifice meter A. Upon leaving orifice meter A, the cooling water flow divides with part of it passing through the calorimeter and the remainder passing through by-pass line B. The valve E permits some regulation of the amount of cooling water which passes through the calorimeter. Orifice meters A and B are thin plate orifice meters with vena contracta pressure taps located in accordance with ASME standards. The pressure drops across orifice meters A and B are measured with mercury-water manometers. Calibration curves for the two orifices are included in the Appendix. After leaving the calorimeter the cooling water is dumped to the atmosphere.

The arc torch control console has a thin plate orifice for measuring the primary gas flow rate. The pressure drop across the thin plate orifice is indicated on a Barton differential pressure meter with a 0-100 per cent scale. Calibration curves for argon gas flowing through the 0.1140 inch diameter orifice are included in the Appendix for several metering pressures. The secondary gas flow rate is measured with a 0-30 SCFH Dwyer rotometer.

The test section pressure is measured with a Crosby vacuum-pressure

meter with a range from 30 inches Hg. vacuum to 15 psig. A calibration curve for the vacuum-pressure meter is included in the Appendix.

The amount of potassium seed material added to the argon gas flow is adjusted by controlling the speed of the motor driving the piston in the positive displacement seeding mechanism. The drive motor RPM is measured with a Type B low speed Hasler Speed Indicator. Adjustment of the motor speed with the Heathkit motor speed controller allows the metering rate of potassium to be changed.

Ten copper-constantan thermocouples were used to measure the cooling water temperature, primary and secondary argon temperatures, and the potassium holder temperature. A common reference junction at 32°F was used for the ten thermocouples. The output potential of the thermocouples was fed through a Leeds and Northrup thermocouple switch and read with a Leeds and Northrup Millivolt Potentiometer Model 8686. A sketch of the thermocouple circuit is shown in Figure (10). The ten thermocouples were calibrated against a standard thermocouple certified by the National Bureau of Standards. Calibration curves for four of the thermocouples are included in the Appendix.

The test gas temperature was measured by two independent means. A 0.060 inch diameter tungsten wire was inserted into the gas stream at a point between the test electrodes and the tip of the tungsten wire was viewed with a Leeds and Northrup Optical Pyrometer. This method provided an almost instantaneous means of determining gas temperature. The Leeds and Northrup Optical Pyrometer was calibrated with a Mole-Richardson Type 2731 Molarc Lamp. The calibration procedure and calibration data are included in the Appendix. The calorimeter provided a second means for the determination of the gas temperature at the exit of the test section. By

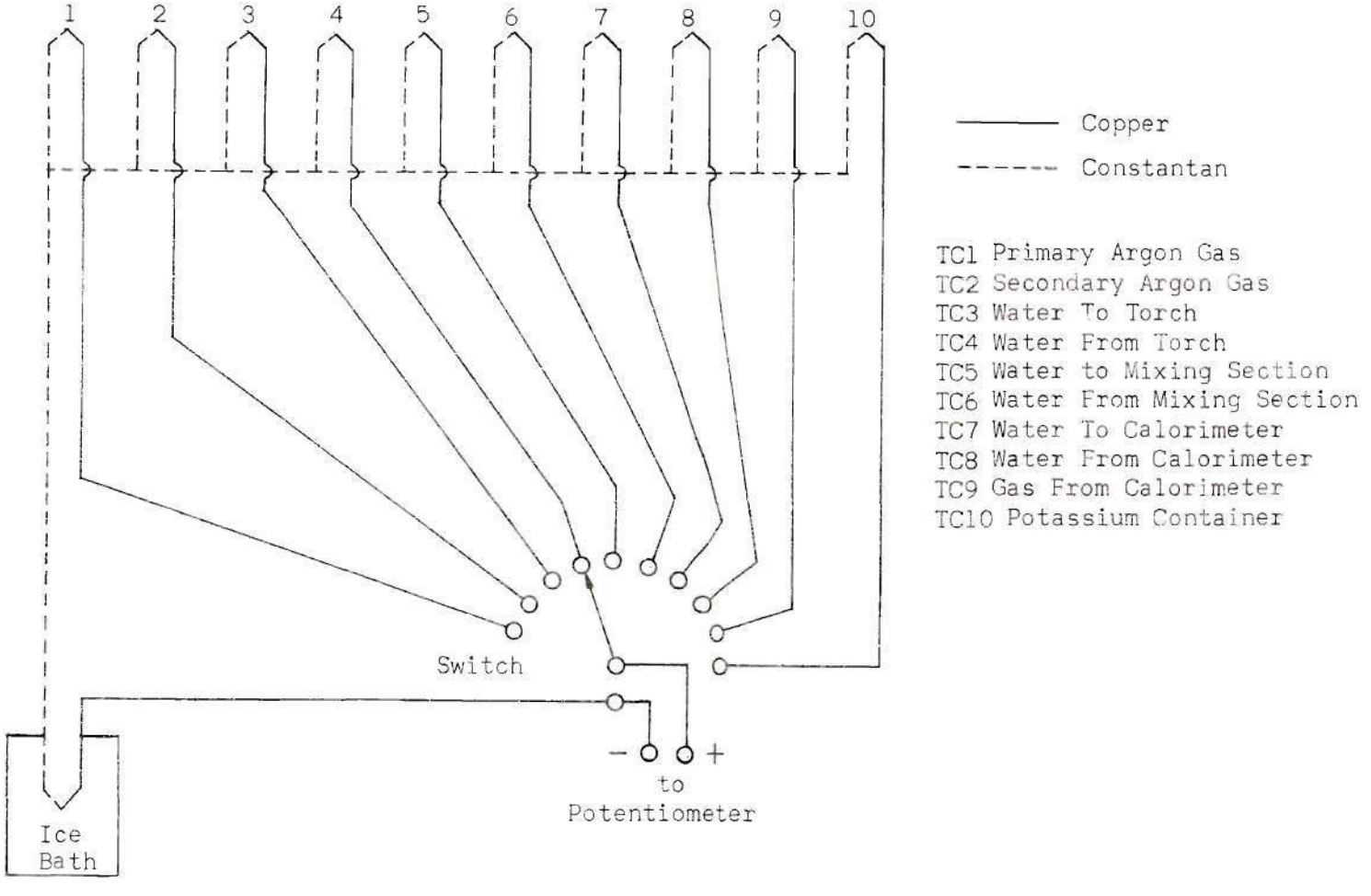

Figure 10. Thermocouple Circuit.

measuring the heat input to the cooling water and the gas temperature leaving the calorimeter, the gas temperature entering the calorimeter can be determined. There is a slight lag time before the calorimeter reaches steady state operation and for this reason calorimeter temperature readings were not made immediately after the test section had attained steady state. Initially, a heat balance was to have been made upstream of the test section; however, it was necessary to use an uncooled mixing chamber which prevented making such a heat balance.

The voltage-current characteristic of the test section was obtained by applying a steady DC voltage between the electrodes and measuring the total current in the external circuit and the voltage difference between two probes inserted in the flow. The DC voltage source was twelve 12 volt storage batteries. The test section voltage could be varied by changing the number of batteries used or by changing the setting on the 3.25 ohm General Electric field rheostat which was in series with the batteries. The current in the circuit was determined by measuring the voltage drop across a 100 millivolt 150 ampere Esterline Angus shunt Serial No. 160 273.

Two different techniques were used to record the voltage-current characteristic. In the first method after applying the test voltage to the electrodes, the resistance of the field rheostat was varied from 3.25 to 0 ohms while the millivolt output of the shunt and the voltage difference between the two probes were being recorded on a Moseley Model 7100BM Strip Chart Recorder having two Model 17501A Plug-In Modules. To eliminate high frequency noise from the output traces, it was necessary to use two high frequency filters on the signals before sending them to

the recorder. A sketch of the set-up used in this measurement technique is shown in Figure (11). It was felt that the continuously applied voltage used in this technique was leading to undesirable Joule heating of the neutral gas, and for this reason a pulse technique was also used.

In the pulse technique, the probe voltage difference and the millivolt output of the shunt were measured continuously during the first 200 μ seconds after the test voltage was applied to the electrodes by a Type 555 Dual-Beam Tektronix oscilloscope with Type G and Type CA Plug-In Units. Using a time base of 50 μ sec/cm, both channels were triggered by the first voltage input from the voltage probes. Pictures of the oscilloscope traces were taken with a Polaroid Land Camera using 3000 speed type 47 film. To eliminate the high frequency noise from the shunt millivolt output, it was necessary to use a high frequency filter. A sketch of the set-up used in this technique is shown in Figure (11).

Test Procedure

The cooling water and the water pump are turned on and the cooling water flow rates are adjusted to get the desired flow through the arc torch and calorimeter cooling circuits. It is necessary that the cooling water pressure at the entrance to the arc torch control console be maintained at at least 90 psig since the arc torch will not operate below this pressure. The temperatures of the cooling water entering and leaving the calorimeter are monitored on a strip chart recorder and allowed to reach a steady state value before continuing.

The primary and secondary argon gas supply bottles are opened and the desired supply pressures are set. The vacuum pump is started and argon flow rates are set to the desired values. The primary argon flow

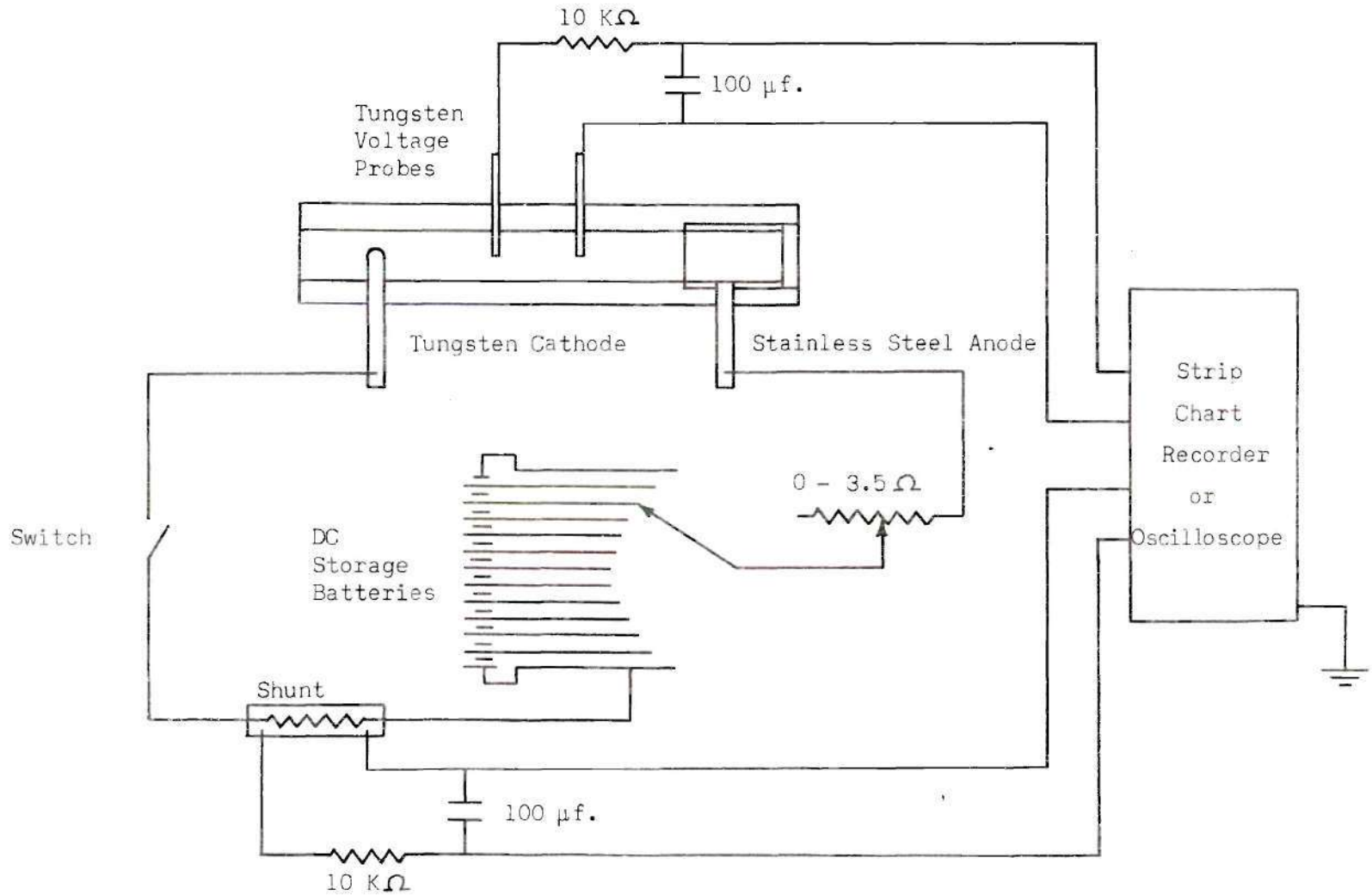

Figure 11. Electrical Measurement Circuit.

rate is adjusted at the arc torch control console and the secondary argon flow rate is adjusted at the rotometer. After establishing the gas flow rates at the proper test section pressure, the primary flow rate is increased to a minimum of 0.01 lbm/sec since this amount of flow is needed to start the arc torch. The gas flow and vacuum pump are stopped until time to test.

The nichrome heating elements on the potassium syringe holder and the secondary argon heating section are set to get the desired temperatures. The inside of the potassium syringe holder is maintained at about 200°F which is sufficient to keep the potassium in the liquid state. The secondary argon gas is heated to approximately 400°C in the nichrome heating section.

Two or three grams of potassium are loaded in the 10cc Luer-Lok syringe according to the procedure outlined in the Appendix and the syringe is placed into the syringe holder. The positive displacement drive mechanism is connected to the syringe piston and secondary argon gas is passed by the needle on the syringe.

The vacuum pump is started and the torch is ignited from the control console with the current control rheostat at the minimum setting. The starting current for the torch should not exceed 100 amps. The primary argon gas flow rate is adjusted to 3 gms/sec. and the current control rheostat is set to give the proper current. As soon as the test section temperature has reached a steady state value, the potassium seed mechanism is started and adjusted to give the desired potassium seed fraction. The gas temperature is measured with the optical pyrometer prior to applying a test voltage across the test section electrodes.

Depending on the test being conducted, the voltage and current readings are recorded on the strip chart recorder or the oscilloscope.

On tests using the strip chart recorder, the recorder is turned on early enough to allow sufficient warm up time before the test and a calibration check is performed. A choice of the DC voltage to be used is made from the battery bank and the field rheostat is set at 3.25 ohms. The switch is closed applying the voltage across the test section electrodes and initiating the gas discharge. The field rheostat is varied slowly from 3.25 ohms to 0 ohms and back to 3.25 ohms. The switch is opened and the next test is ready to be run.

When the oscilloscope is used, sufficient warm up time is allowed and the gain of each channel is checked with the amplitude calibrator. The DC voltage and the field rheostat resistance to be used are set. Both beams of the oscilloscope are operated from the same time base unit operating at a 50 μ sec/cm sweep speed. The time base unit is operated on the single sweep mode with both beams being triggered with the initial probe voltage input. The camera lens opening is set at f/5.6. The camera shutter is opened and the oscilloscope is triggered manually to get base-line traces of the two beams. The sweep is reset and the switch is closed initiating the discharge. The probe voltage input to the oscilloscope triggers both beams of the oscilloscope giving voltage-current traces for the first 450 μ seconds of the discharge. The camera shutter is closed having been open for a 5 second time exposure. The picture is developed and additional data points are obtained in the same manner.

Joule Heating Effect

During the course of the tests, it became apparent that the continuously applied test voltage, which was used initially, was leading to

significant Joule heating of the neutral gas. To account for this effect, which becomes important at high current densities, a calibration test was made with the calorimeter to determine the increase in gas temperature as a function of the electrical energy input j^2/σ. The data points were obtained by applying a test voltage and allowing sufficient time for the calorimeter to reach steady state. Because of the relatively slow response time of the calorimeter, data points at high current densities could not be obtained before overheating the test section. A plot of the increase in gas temperature as a function of j^2/σ is shown in Figure (12). The high current density point was obtained before the calorimeter had completely achieved steady state.

To obtain a theoretical curve which includes the Joule heating of the neutral gas a value of j^2/σ is calculated for a point on the theory curve. This j^2/σ is used in Figure (12) to arrive at an increase in gas temperature due to Joule heating of the neutral gas. Using this increased gas temperature, a new value of σ is obtained for the j value of the initial point. This procedure is followed for a sufficient number of points to determine a new theoretical curve which includes the Joule heating of the neutral gas. This new theoretical curve is shown in Figure (13) for a typical run condition.

Data Reduction

The scalar electrical conductivity was calculated from the experimentally obtained voltage-current characteristic of the test section by assuming that Ohm's Law in the form $\vec{j} = \sigma\vec{E}$ was valid for each test condition.

The current density, j, was obtained from the measured total current

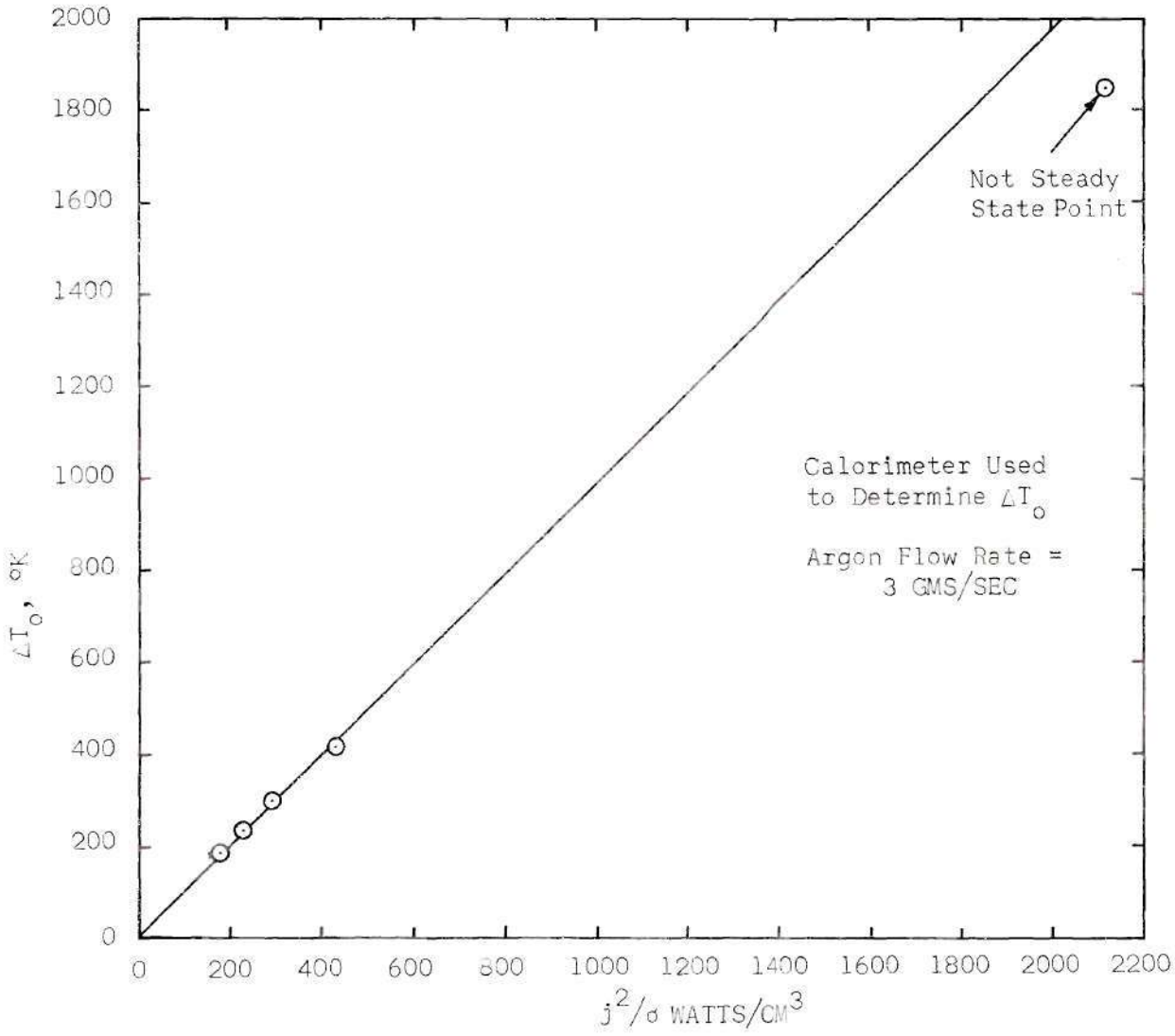

Figure 12. Joule Heating Calibration Curve.

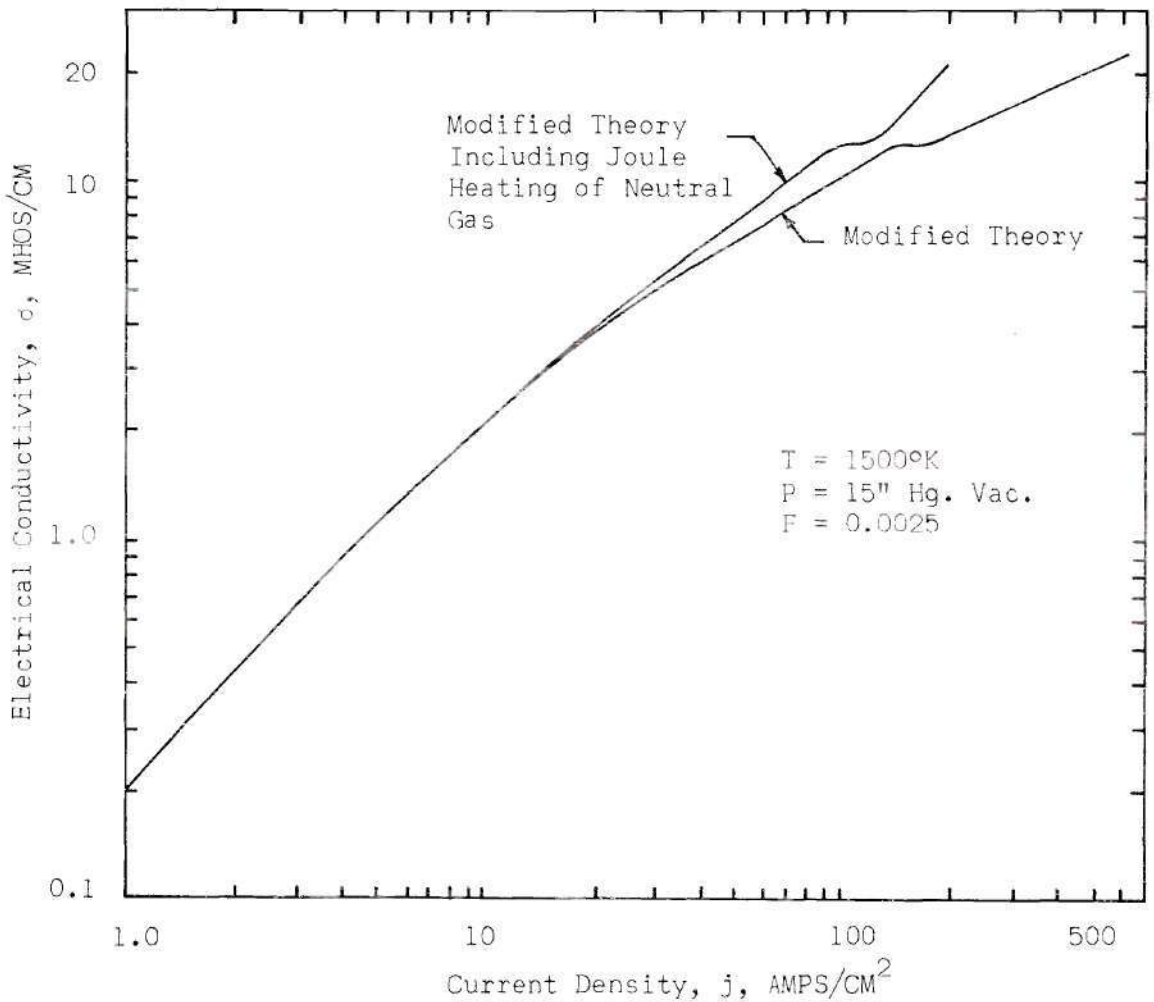

Figure 13. Electrical Conductivity Including Joule Heating of Neutral Gas.

passing through the test section, I, and the cross-sectional area of the test section, A. In this calculation it was assumed that the test discharge filled the entire volume between the test electrodes and did not localize in any one area. For normal discharges this should give an average value for the current density in the test section. Thus, the current density was obtained from the equation:

$$j = \frac{I}{A} \tag{30}$$

The electric field, E, was obtained from the measured potential difference between two voltage probes inserted in the gas stream between the test electrodes, V, and the distance separating these two probes, ℓ. The use of this voltage difference eliminates the sheath effects present on the test electrodes. An indication that the electrode sheath effects were confined to a region very close to the electrodes was obtained by measuring the voltage distribution between the electrodes with 4 test probes. A plot of this voltage distribution for a typical test is shown in Figure (14). Thus, the electric field was obtained from the equation:

$$E = \frac{V}{\ell} \tag{31}$$

The scalar electrical conductivity was obtained from j and E by Ohm's Law:

$$\sigma = \frac{j}{E} = \frac{I\ell}{AV} \tag{32}$$

The total current passing through the test section and the probe voltage difference were obtained directly from data of the strip chart recorder;

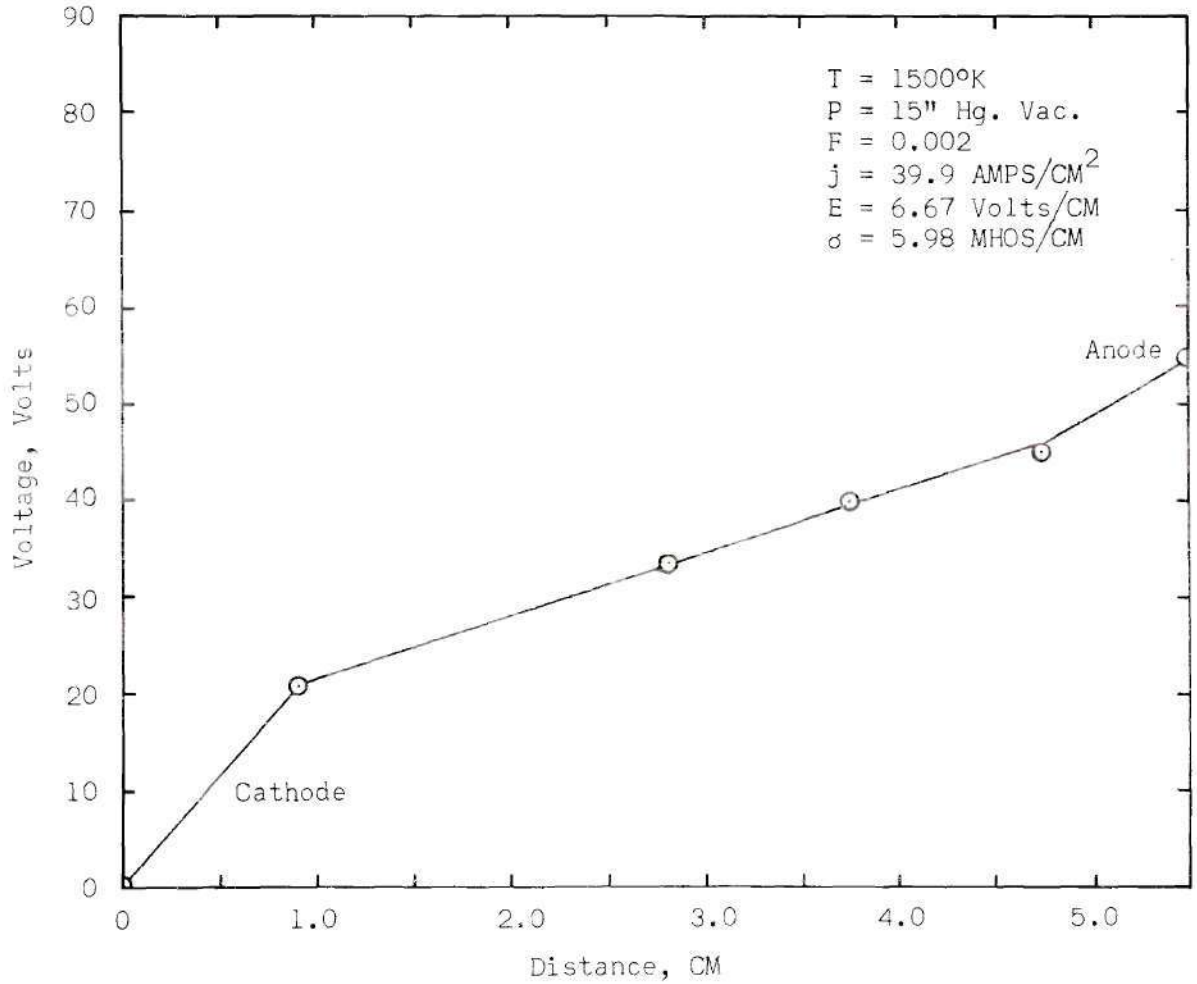

Figure 14. Voltage Distribution Between Test Electrodes.

however, some further comments are required about the oscilloscope data reduction.

To obtain the nonequilibrium value of the electrical conductivity without the effect of Joule heating of the neutral gas, it is necessary to obtain the voltage-current characteristic at the appropriate time. Sufficient time must be allowed for the heating of the electrons and the nonequilibrium ionization to occur. Zukoski, Cool and Gibson (13) have analyzed the response of a plasma to a step function electric field by using the time dependent energy equation. It is shown that the relaxation time for the establishment of the new electron temperature is less than 3 μ sec. and that the relaxation time for the nonequilibrium ionization process is about 20 μ sec. for an electric field of 5 volts/cm. The relaxation time for nonequilibrium ionization decreases with increasing electric field and should therefore be less than 20 μsec. for all of the present data. The relaxation time for the heating of the neutral gas is much longer than for the other relaxations, being of the order of several 100 μsec. before appreciable changes in conductivity result. A plot of the electrical conductivity versus time is shown in Figure (15) for a typical oscilloscope data point. The conductivity of interest here is the leveled out value under 50 μsec. before significant Joule heating of the neutral gas has occurred.

Discussion of Test Results

The electrical conductivity of an argon-potassium plasma has been experimentally determined as a function of current density for gas temperatures from 1500 to 1800°K, gas pressures from 15" Hg. Vac. to atmospheric pressure and potassium seeding fractions from 0.002 to 0.004. A potassium

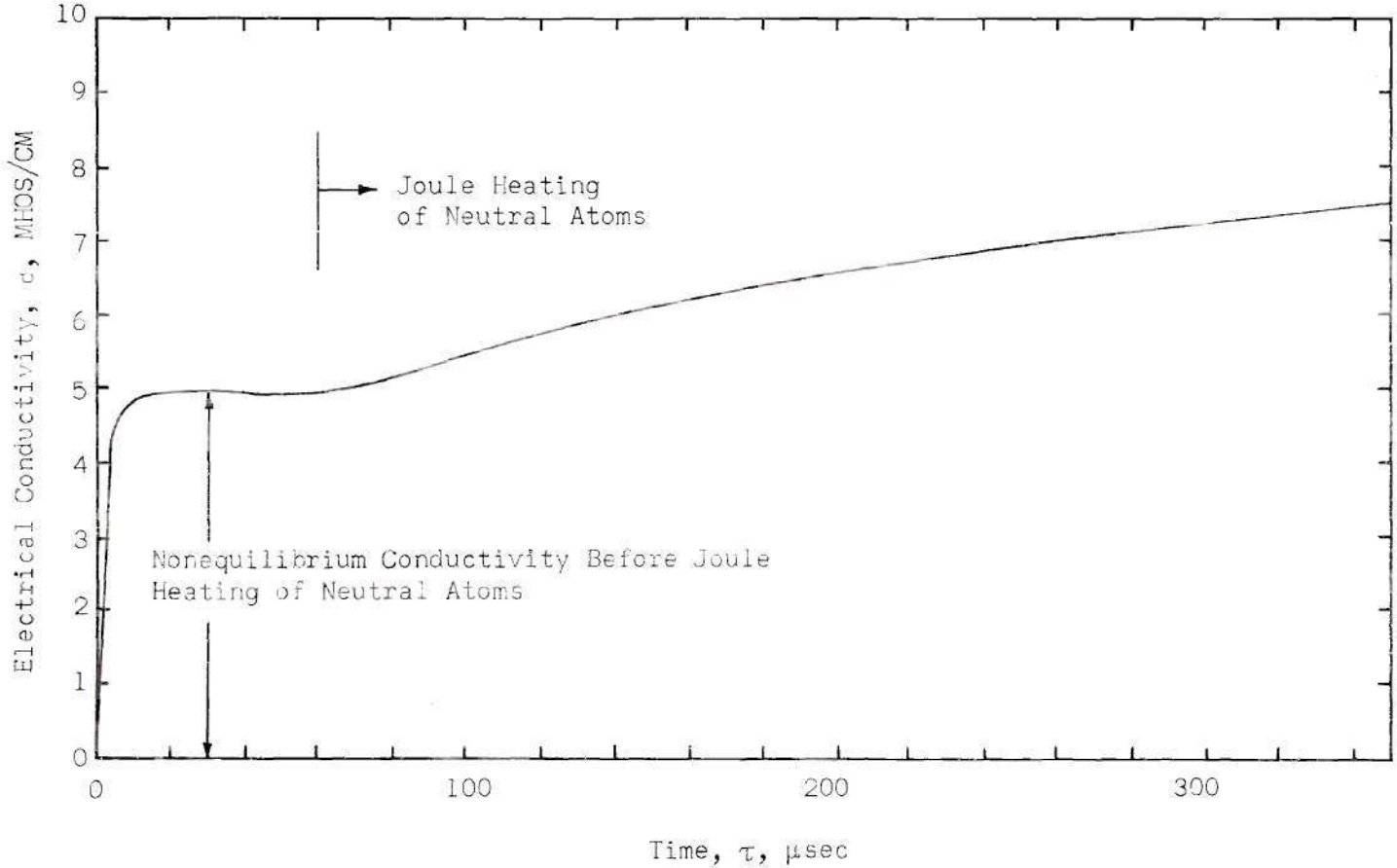

Figure 15. Transient Electrical Conductivity.

seeding fraction of 0.001 was attempted on several tests; however, the positive displacement seeding mechanism gave erratic results for this low seeding rate. The argon flow rate for all of the tests was 3.0 gm/sec. with 90 per cent of the argon flow going through the arc torch and 10 per cent of the argon flow going through the secondary flow system. Electrical conductivity data were obtained by two different methods. The first was a continuous method in which the voltage-current response of the plasma to a slowly changing applied voltage was recorded on a strip chart recorder. The second was a pulse technique in which the transient voltage-current response of the plasma to a constant step voltage input was recorded on an oscilloscope. Duplicate tests were made for the same test conditions to determine if the data were reproducible.

The electrical conductivity data are shown in Figures (16) to (24) for various test conditions. The tests covered a range of current densities from 1.0 to about 180 amps/cm^2 with a corresponding variation in electrical conductivity from 0.2 to about 15 mhos/cm. In each figure, two theoretical curves are shown; the modified theory curve including the effects of argon ionization and radiation loss from the plasma, and the modified theory curve corrected for the Joule heating of the neutral gas. For example, consider Figure (16) which shows three different tests having the same test conditions with the data being obtained with the strip chart recorder. These three tests show that the electrical conductivity data are reproducible. These data show good agreement with the modified theory curve which has been corrected for the Joule heating of the neutral gas. For high current densities, the data agree much better with the modified theory than with the original theory of Shelton and Carlson (16), indicating

the importance of including the ionization of argon in the theoretical calculations of electrical conductivity. The data show a slight plateau in the electrical conductivity at a current density of about 100 amps/cm^2 as predicted by the theory. The value of the electrical conductivity on this plateau is almost entirely a function of the potassium seeding fraction and is therefore a check on the potassium seeding mechanism. Including the Joule heating of the neutral gas does not significantly change the value of the electrical conductivity on the plateau but shifts the plateau to lower current densities.

For high current densities, data obtained with the pulse method using an oscilloscope show better agreement with the modified theory which neglects the Joule heating of the neutral gas than the data obtained with the continuous method. This better agreement of the oscilloscope data with the modified theory is shown in Figures (21) to (24). The pulse method effectively removes the Joule heating of the neutral gas and should therefore show better agreement.

The effect of gas pressure and potassium seeding fraction on the electrical conductivity is shown in Figures (25) and (26), respectively. A decrease in gas pressure results in a higher value of electrical conductivity for a given current density. The data in general show agreement with the effect of pressure predicted by the theory. According to the theory, a lower potassium seeding fraction results in a higher value of electrical conductivity up to the plateau region for the lower seeding fraction after which the higher potassium seeding fraction results in a higher value of electrical conductivity. The experimental data tend to agree with the effect of potassium seeding fraction predicted by the theory for the range of current densities for which data were obtained.

A typical voltage-current trace from the strip chart recorder is

shown in Figure (27). The voltage recorded here is the potential difference between two voltage probes inserted into the gas stream between the test section electrodes and separated by a distance of 0.9 cm. The current trace represents the millivolt output of the 150 amp. shunt used to measure the current. The strip chart recorder was set for a deflection of 0.4 volts/cm on the probe voltage channel and 4 millivolts/cm on the shunt voltage channel. The chart speed was 1.25 cm/sec.

Two typical voltage-current traces from the oscilloscope are shown in Figure (28). The probe voltage difference and the shunt millivolt output are recorded here as a function of time along with a base-line trace for each channel. The two beams were triggered with the initial probe voltage input to the oscilloscope. The oscilloscope was set for a deflection of 5 volts/cm on the probe voltage channel and 50 millivolts/cm on the shunt voltage channel. The sweep speed was 50 μsec/cm. An increase in current and a decrease in probe voltage take place as the gas is heated up. The method of obtaining electrical conductivity data from these oscilloscope pictures is explained in the Data Reduction Section.

The estimated experimental errors in the basic variables are given in Table 1. A detailed error analysis is included in the Appendix.

Table 1. Estimated Experimental Errors in Basic Variables.

Electrical Conductivity	± 7%
Potassium Seeding Fraction	± 7%
Gas Temperature	± 40°K
Gas Pressure	± 1" Hg.

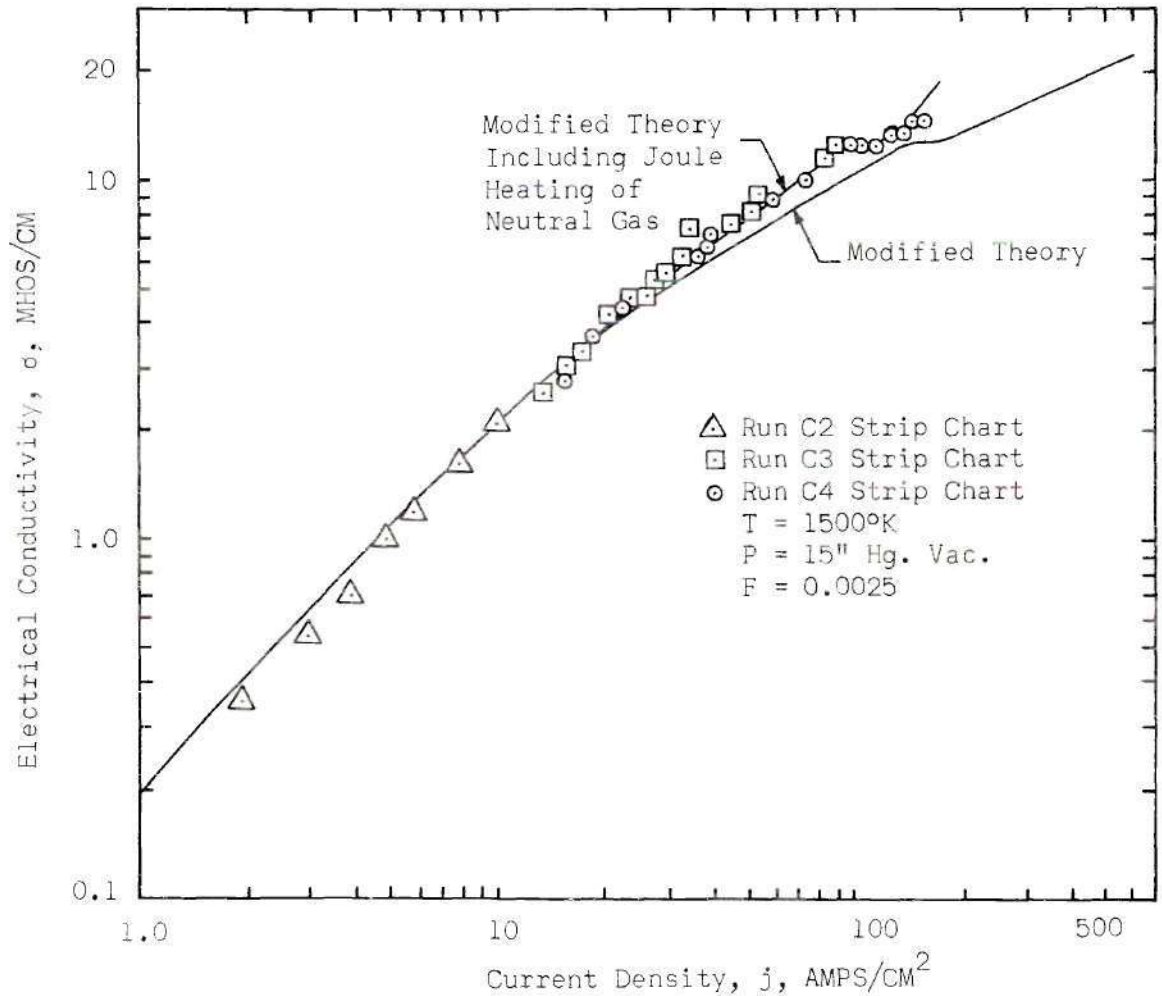

Figure 16. Electrical Conductivity Versus Current Density for T = 1500°K, P = 15" Hg. Vac. and F = 0.0025.

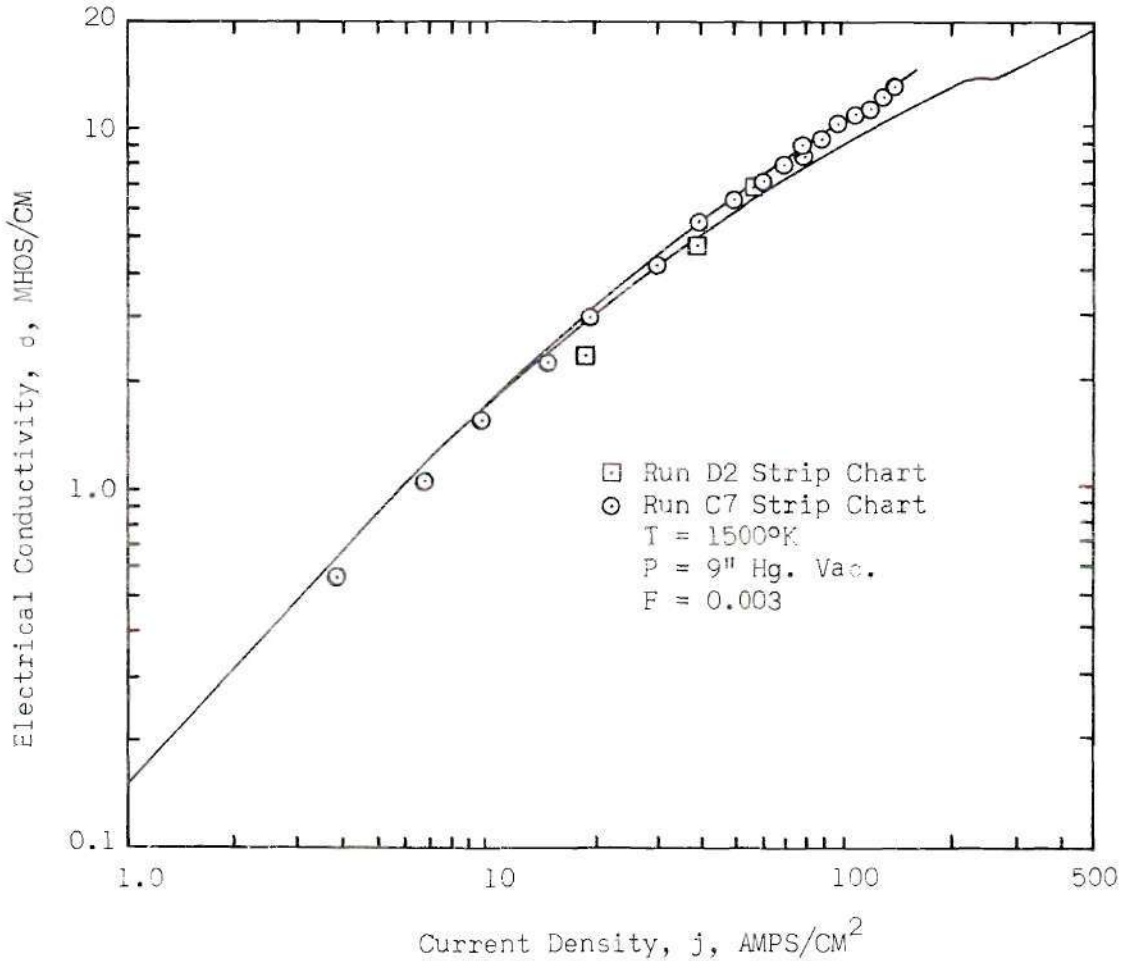

Figure 17. Electrical Conductivity Versus Current Density for T = 1500°K, P = 9" Hg. Vac. and F = 0.003.

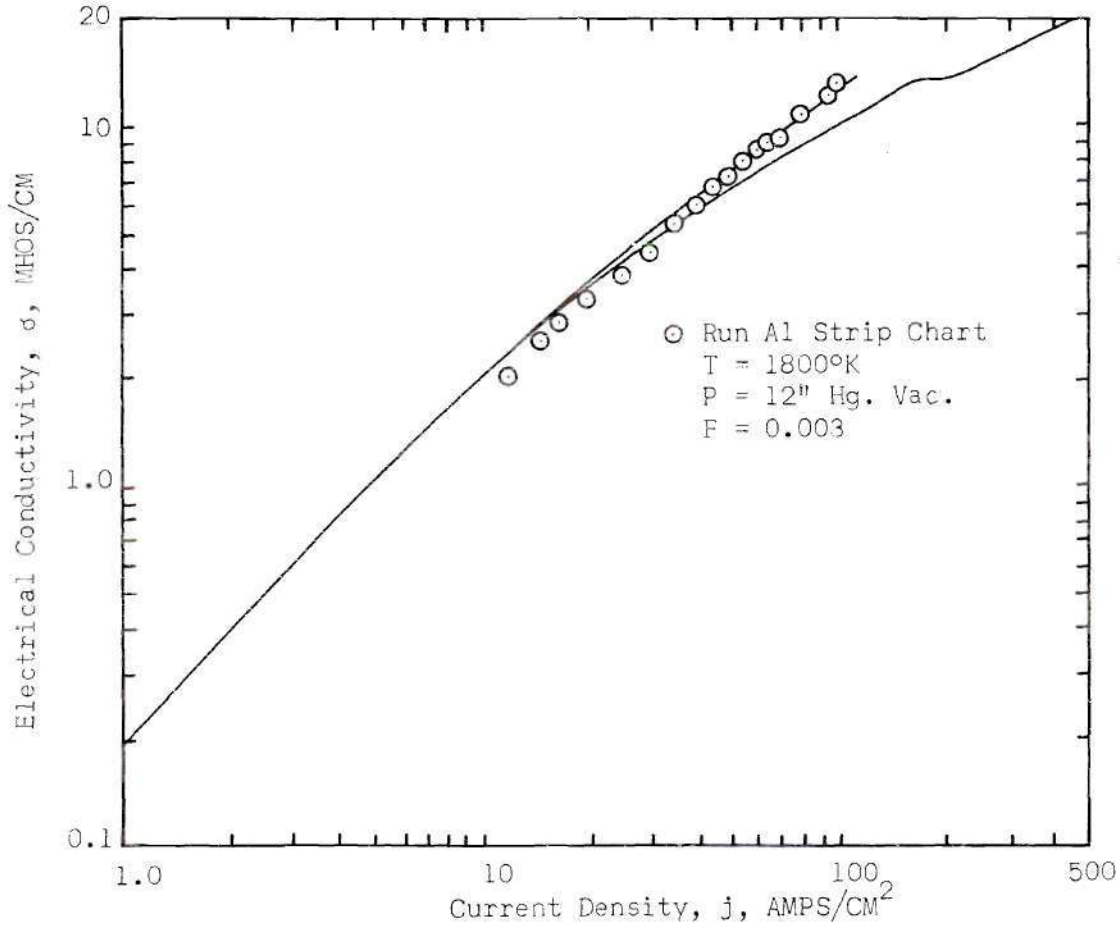

Figure 18. Electrical Conductivity Versus Current Density for T = 1800°K, P = 12" Hg. Vac. and F = 0.003.

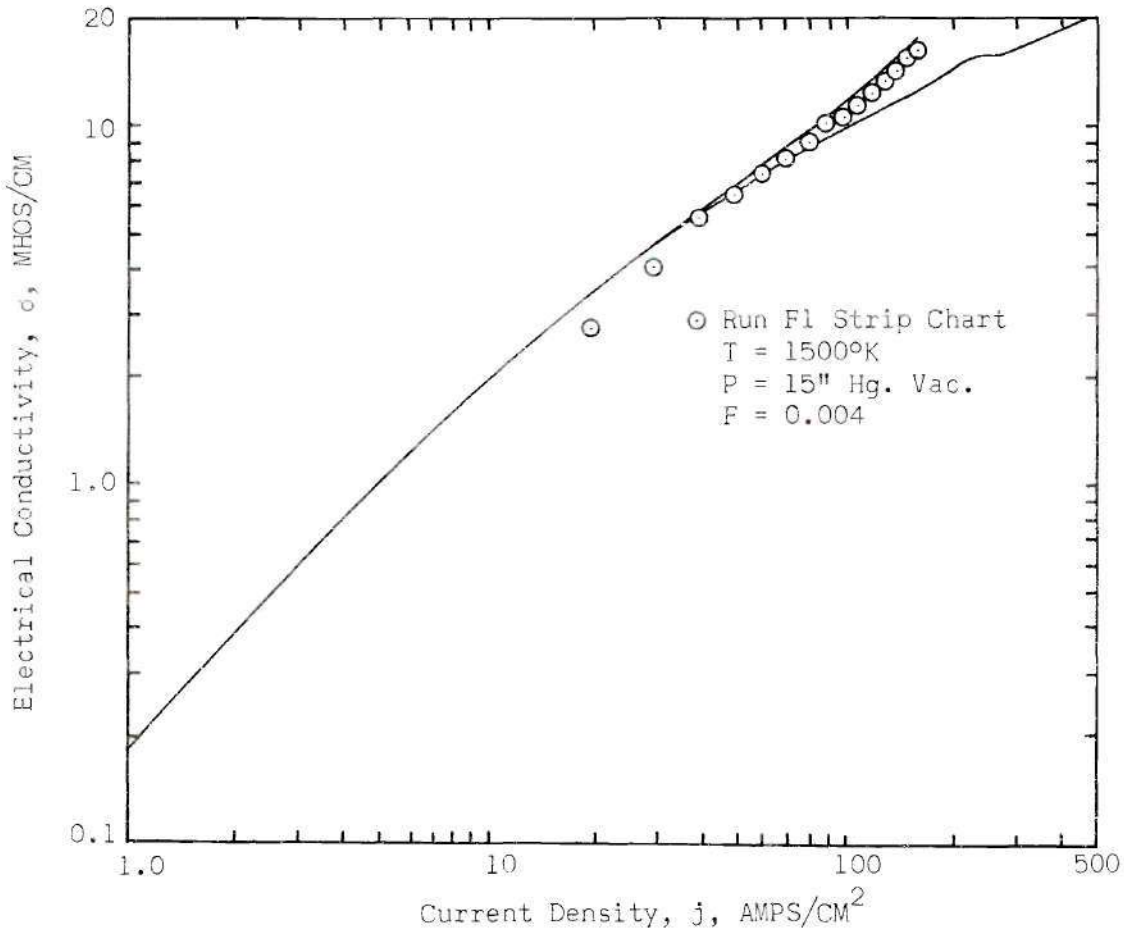

Figure 19. Electrical Conductivity Versus Current Density for T = 1500°K, P = 15" Hg. Vac. and F = 0.004.

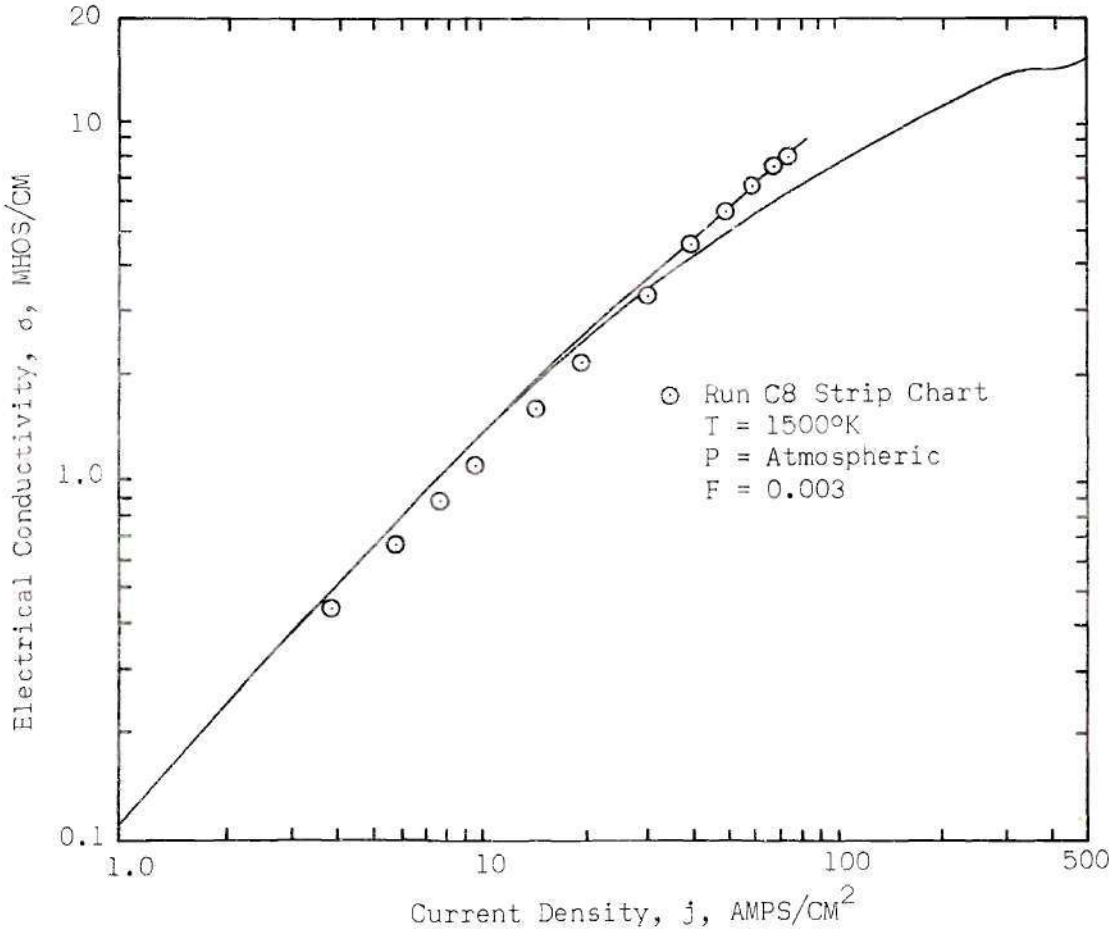

Figure 20. Electrical Conductivity Versus Current Density for T = 1500°K, P = Atmospheric and F = 0.003.

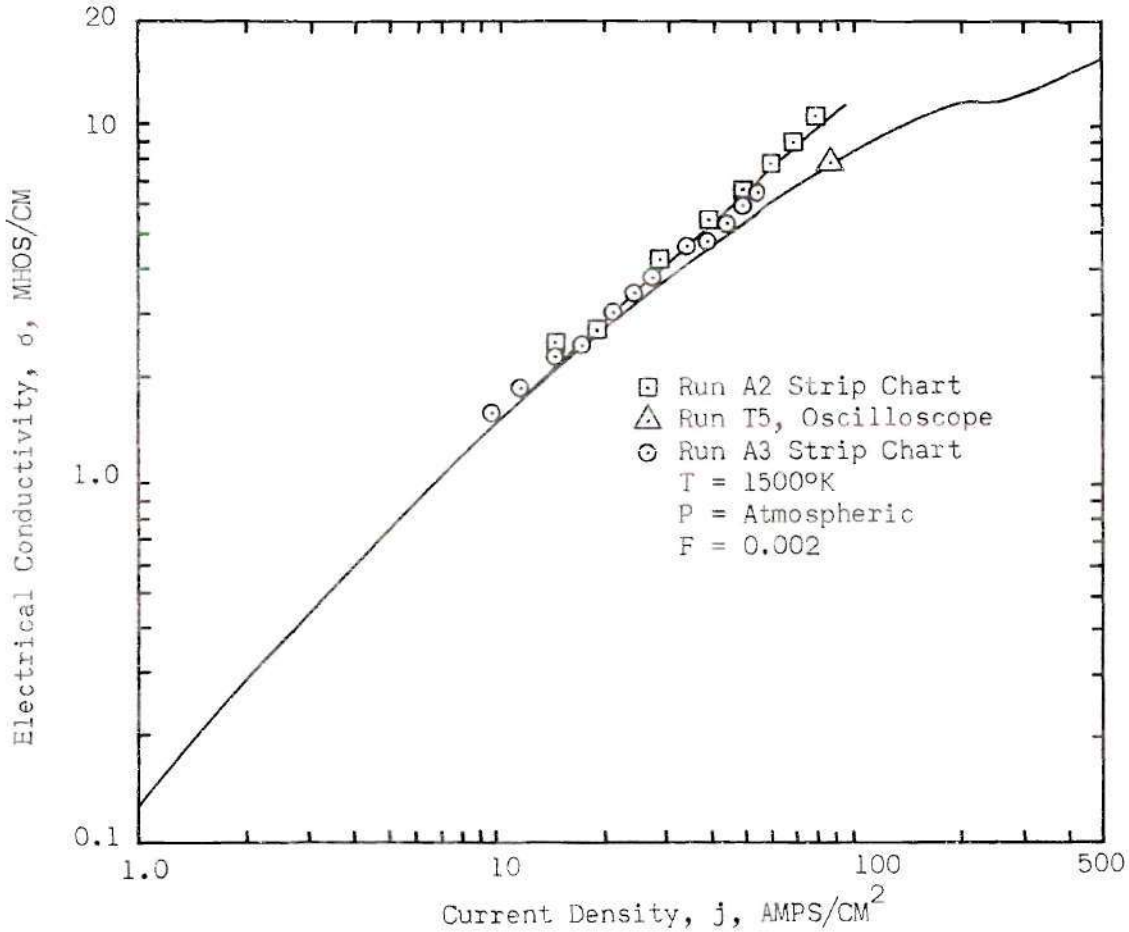

Figure 21. Electrical Conductivity Versus Current Density for T = 1500°K, P = Atmospheric and F = 0.002.

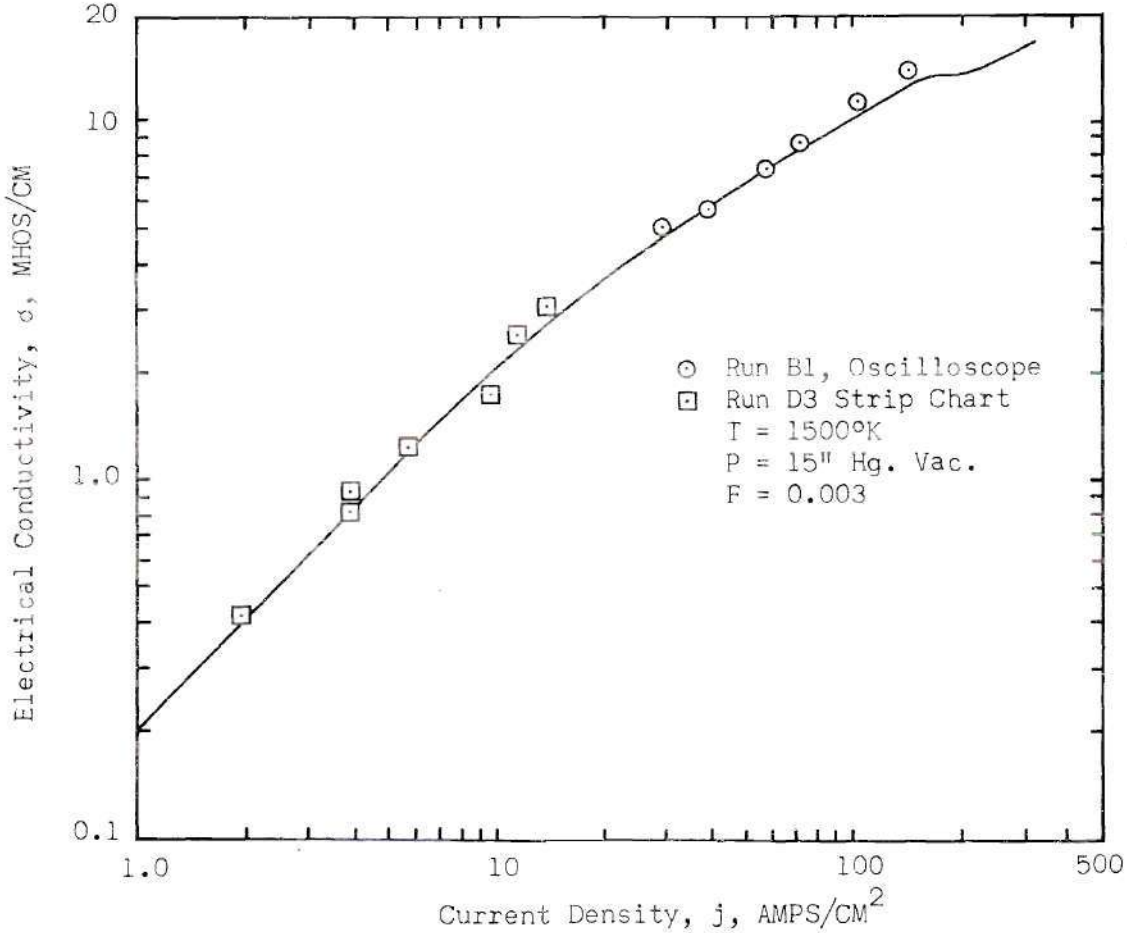

Figure 22. Electrical Conductivity Versus Current Density for T = 1500°K, P = 15" Hg. Vac. and F = 0.003.

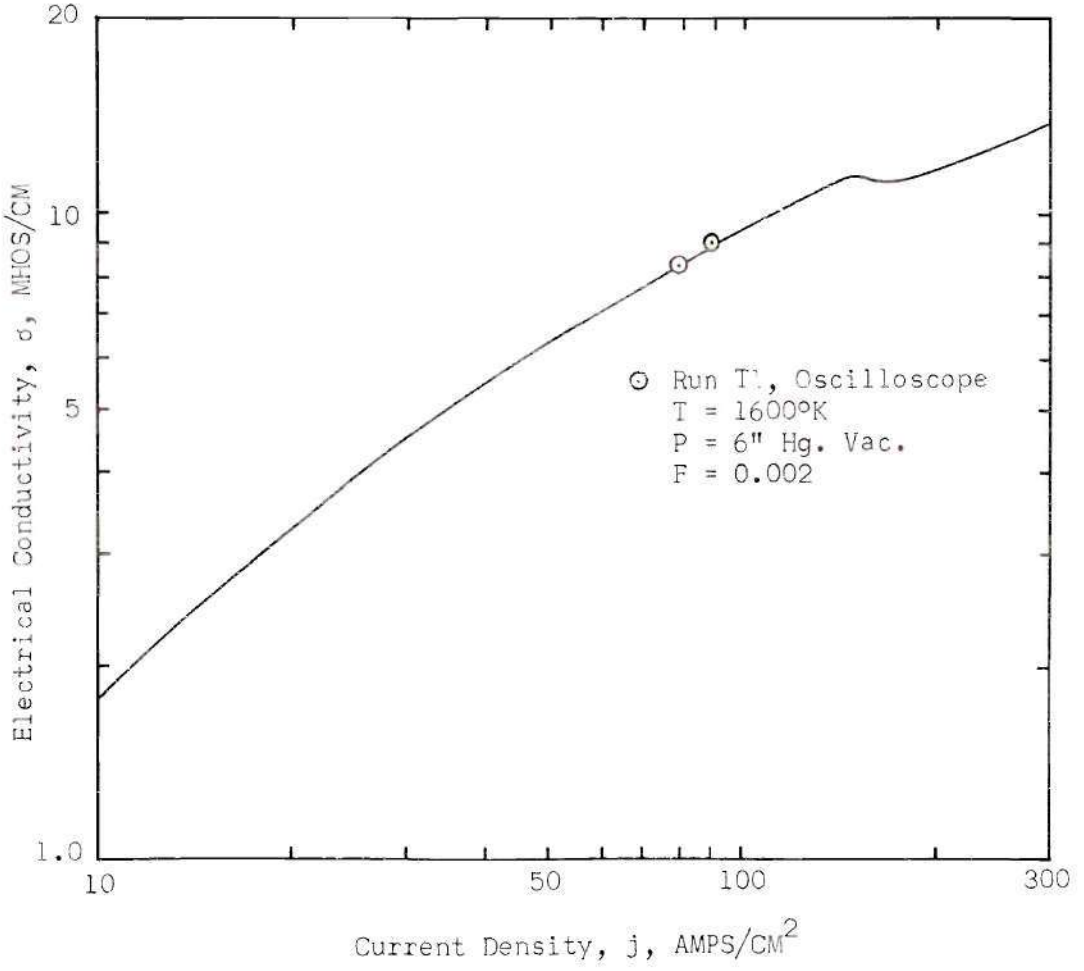

Figure 23. Electrical Conductivity Versus Current Desnity For T = 1600°K, P = 6" Hg. Vac. and F = 0.002.

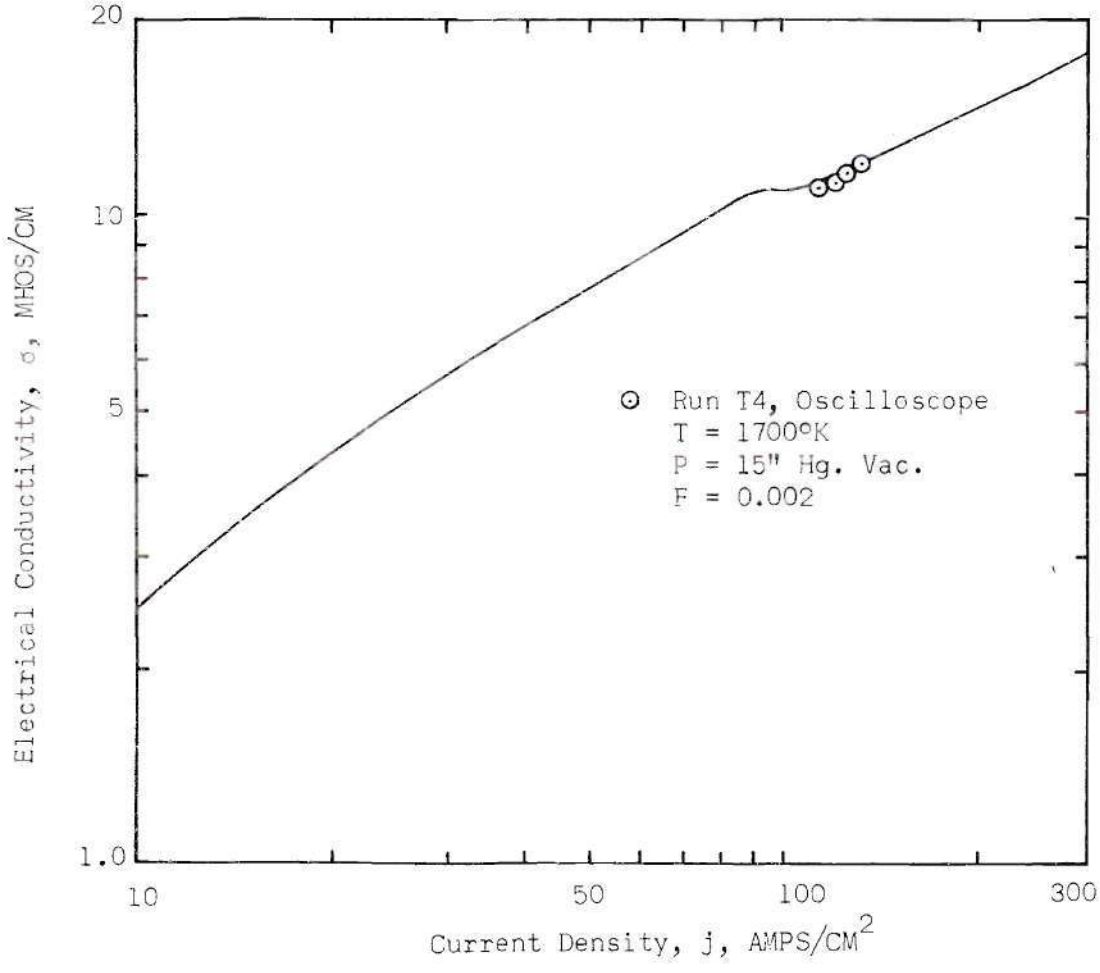

Figure 24. Electrical Conductivity Versus Current Density for T = 1700°K, P = 15" Hg. Vac. and F = 0.002.

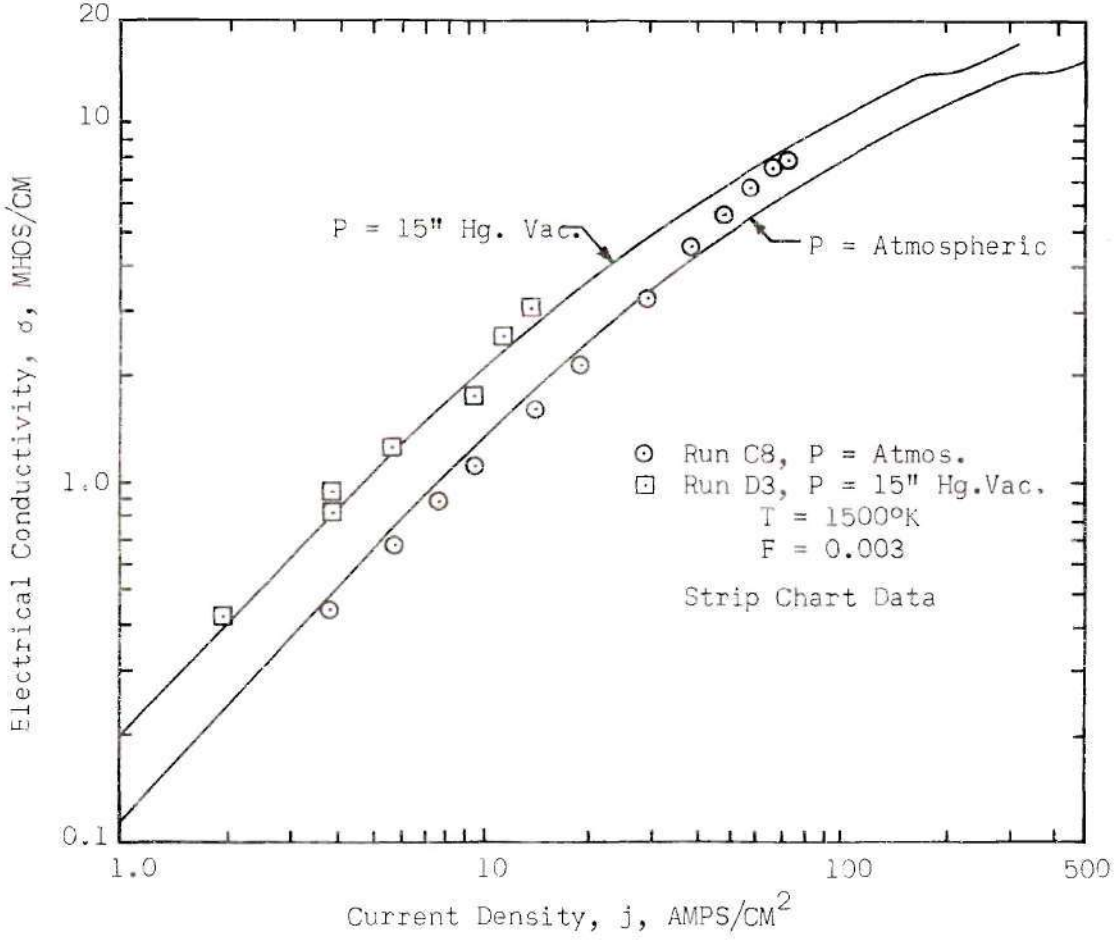

Figure 25. Effect of Gas Pressure on Electrical Conductivity.

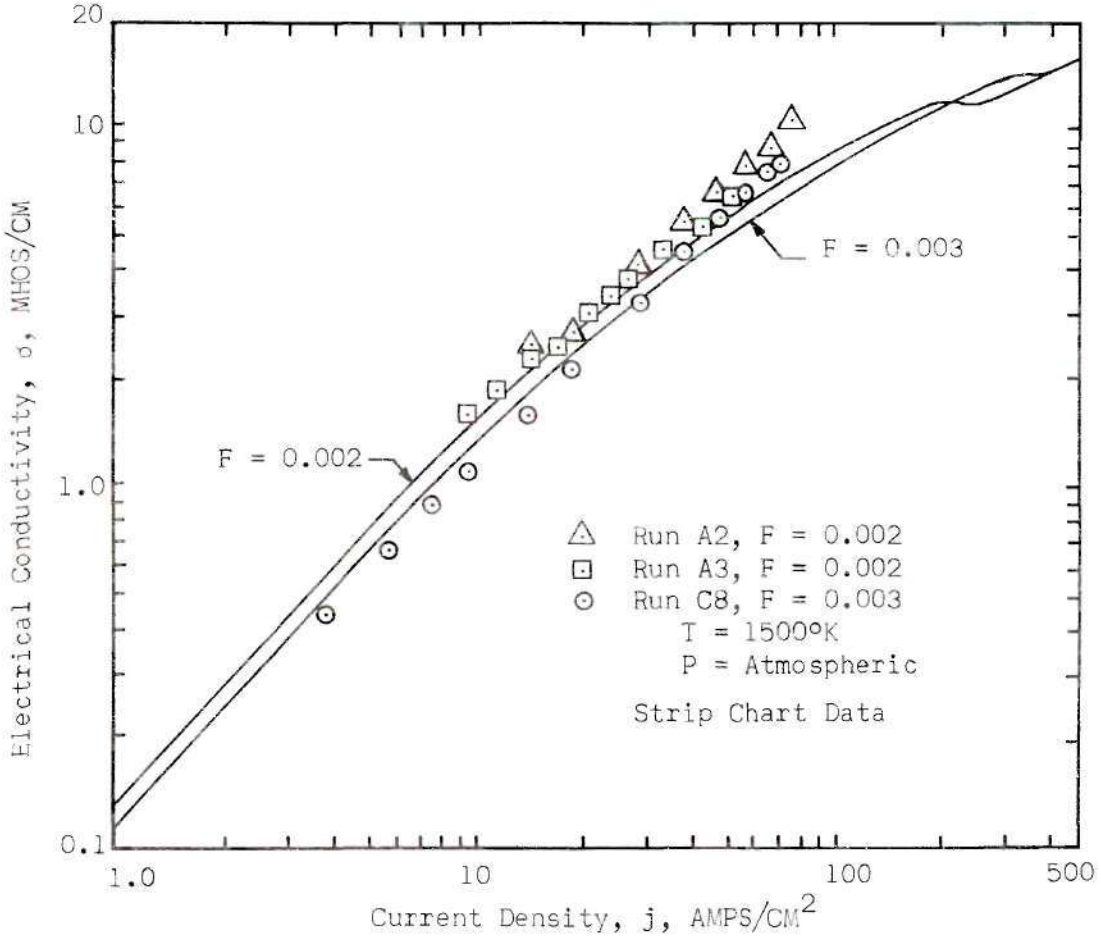

Figure 26. Effect of Seeding Fraction on Electrical Conductivity.

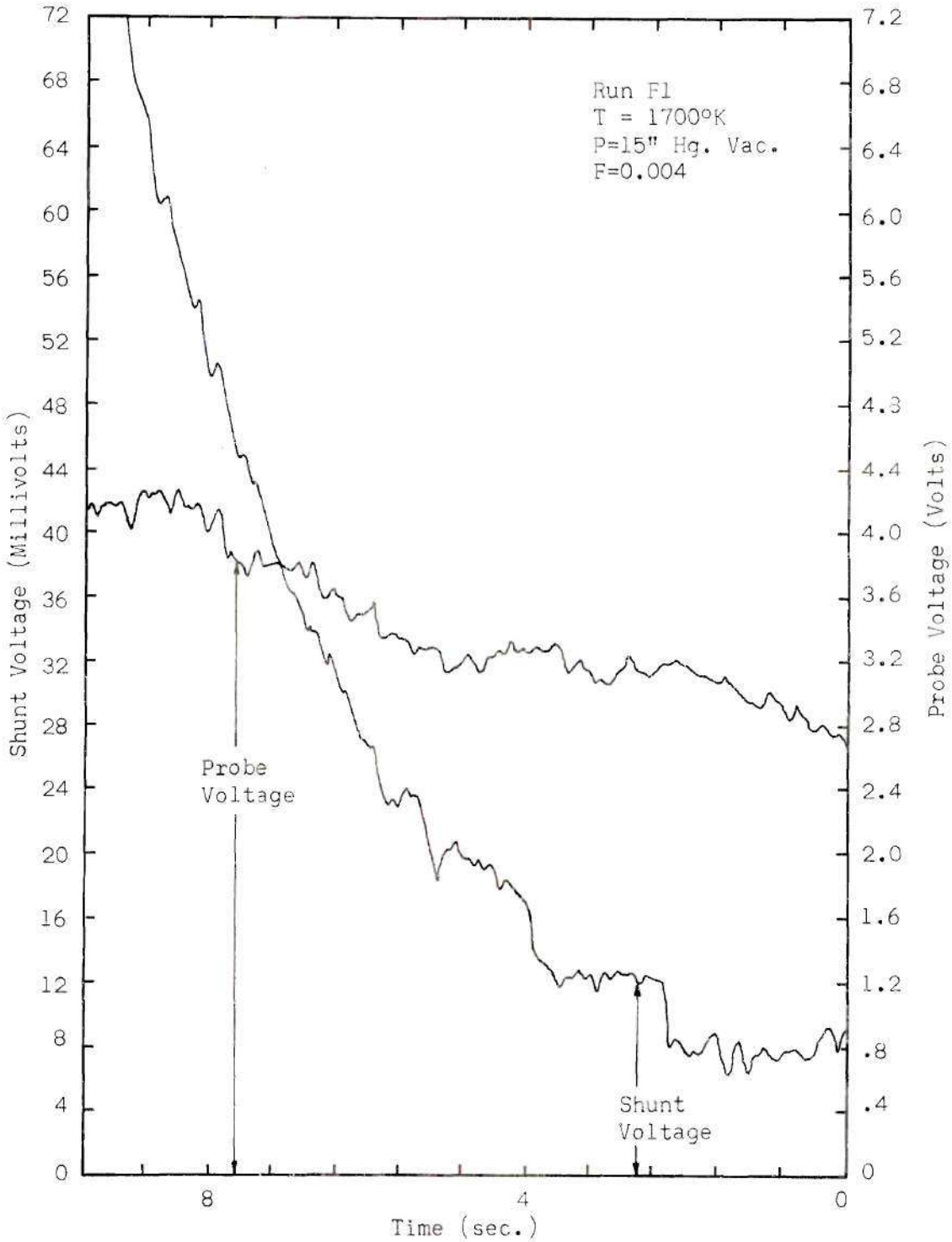

Figure 27. Typical Voltage-Current Trace from Strip Chart Recorder.

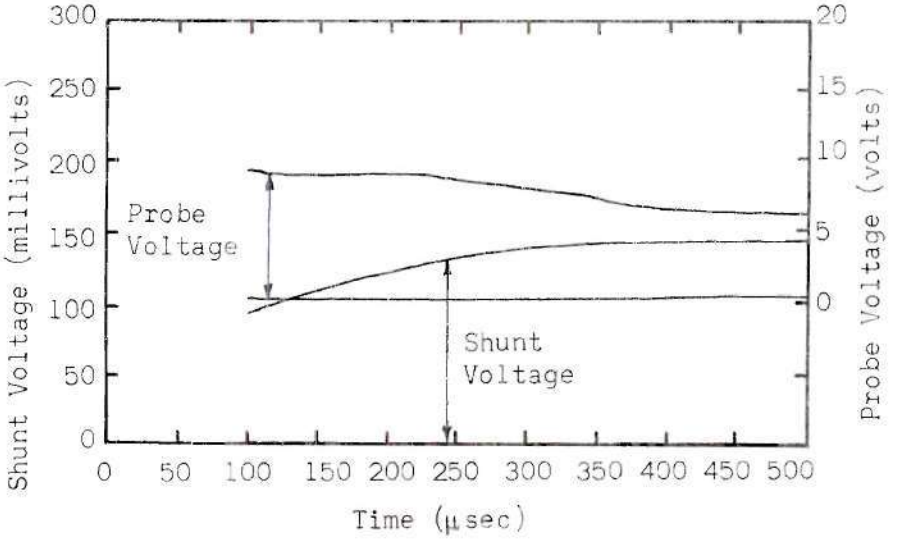

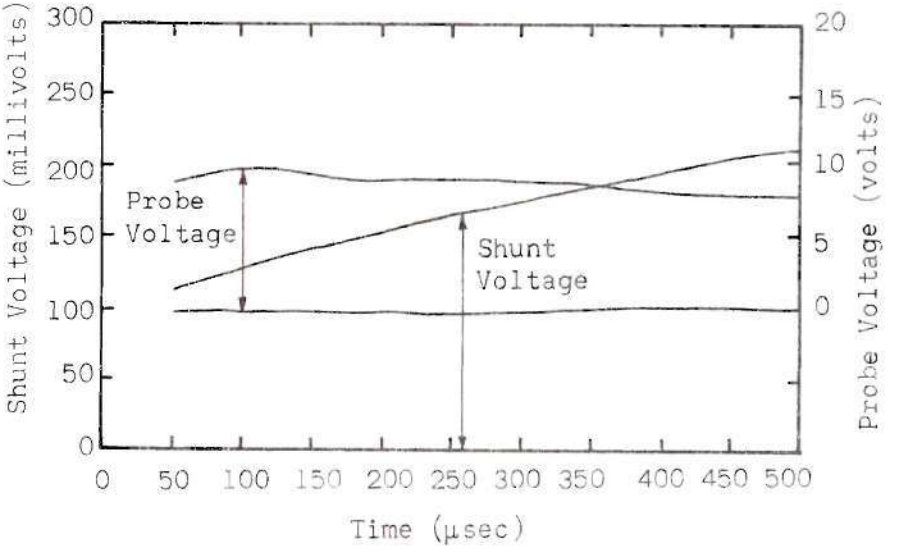

Figure 28. Typical Voltage-Current Traces from Oscilloscope.

CHAPTER IV

CONCLUSIONS AND RECOMMENDATIONS

The experimental electrical conductivity data obtained in these tests show good agreement with the Shelton and Carlson theory (16) when the theory is modified to include the effects of argon ionization and radiation loss from the plasma. For low current densities ($\sim j \leq 80$ amps/cm^2 for the tests made), the argon ionization is insignificant because only a very small number of electrons have high enough energies to ionize an argon atom. For high current densities ($\sim j > 80$ amps/cm^2 for the tests made), argon ionization significantly changes the shape of the electrical conductivity curve. For most test conditions, the peak in the electrical conductivity predicted by the original theory is reduced in the modified theory to a plateau region of constant electrical conductivity followed by a region of increasing conductivity. The effects of gas pressure and potassium seeding fraction on the electrical conductivity were verified by the experiment data.

It is felt that the modified Shelton and Carlson theory is an adequate theory of electrical conductivity for seeded gases over a wide range of current densities; however, some further experiments could lead to a better understanding of the theory. Measurements of the electron temperature as a function of the current density for current densities up to about 200 amps/cm^2 would provide a good check of the energy equation used in the theory. Further experimental work using other seeded gas systems with emphasis placed on the pulse technique for obtaining

data would help complete the work on the electrical conductivity of seeded gases.

APPENDIX

APPENDIX

Optical Pyrometer Calibration

The Leeds and Northrup Optical Pyrometer, which was used to determine the gas temperature, was calibrated using a Mole-Richardson Type 2731 Molarc Lamp burning 1/4 inch Grade SPK positive electrode and 1/8 inch Grade AGKS negative electrode. It has been determined that the anode of this arc has a temperature of 3803 ± 20°K when operated under the conditions given in Reference (26). To obtain temperatures in the range of interest for the electrical conductivity tests, a series of Mole-Richardson Filter Glasses (Serial No. 45) were used in conjunction with the lamp. The filter glasses have been tested by the National Bureau of Standards and the percentage uncertainty in the temperature reading specified. The pyrometer was calibrated by the same person who made the majority of the gas temperature readings with the pyrometer during the tests. A series of pyrometer readings was made using the 1300°K, 1800°K and 2300°K filter glasses with the following results:

Table 2. Optical Pyrometer Calibration.

Filter Glass Used	Pyrometer Readings		
	No. Readings	$< T >$	$\bar{\sigma}$
1300 ± 12°K	5	1261.4°K	4.2°K
1800 ± 20°K	10	1745.7°K	7.6°K
2300 ± 26°K	10	2215.1°K	12.6°K

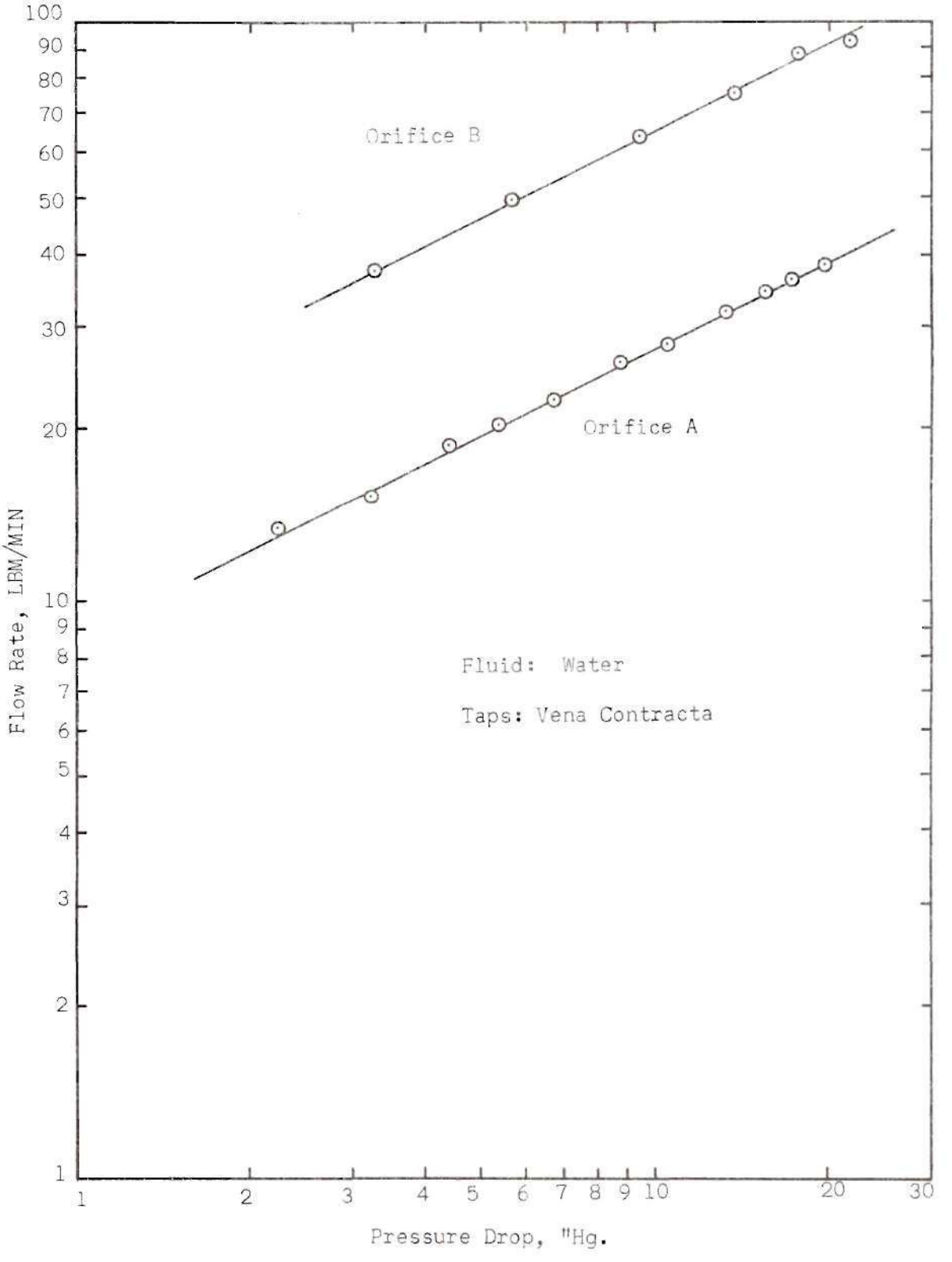

Figure A-1. Water Orifice Meter Calibration Curves.

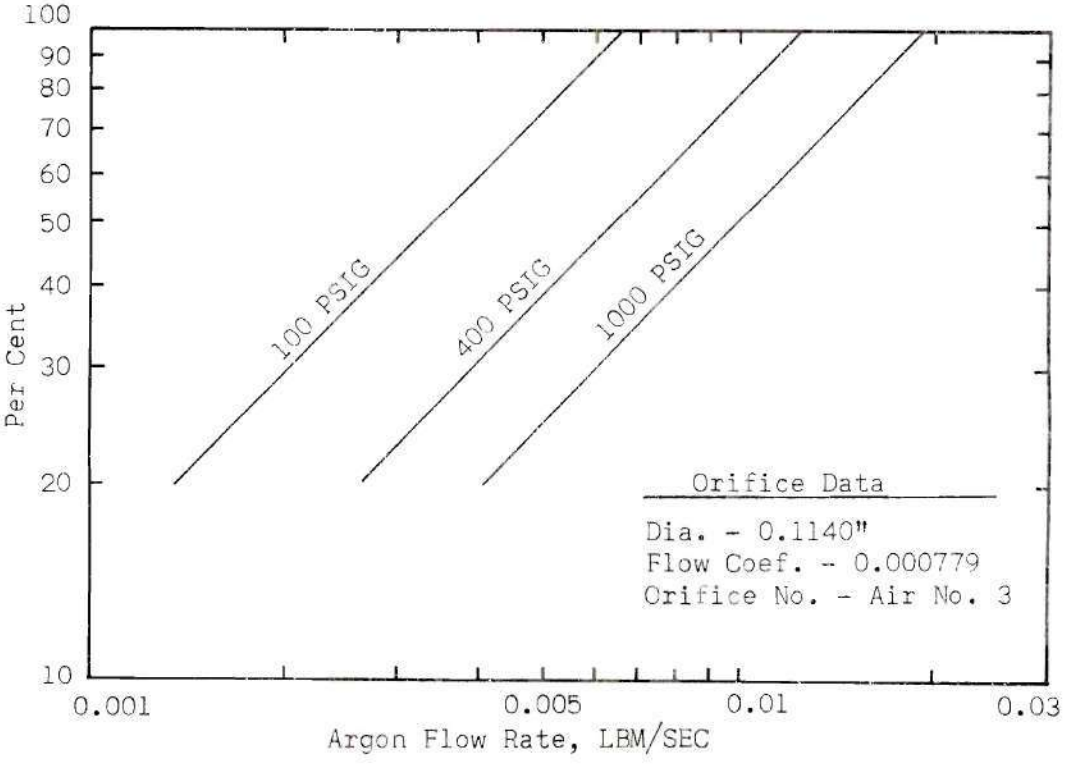

Figure A-2. Argon Orifice Meter Calibration Curves.

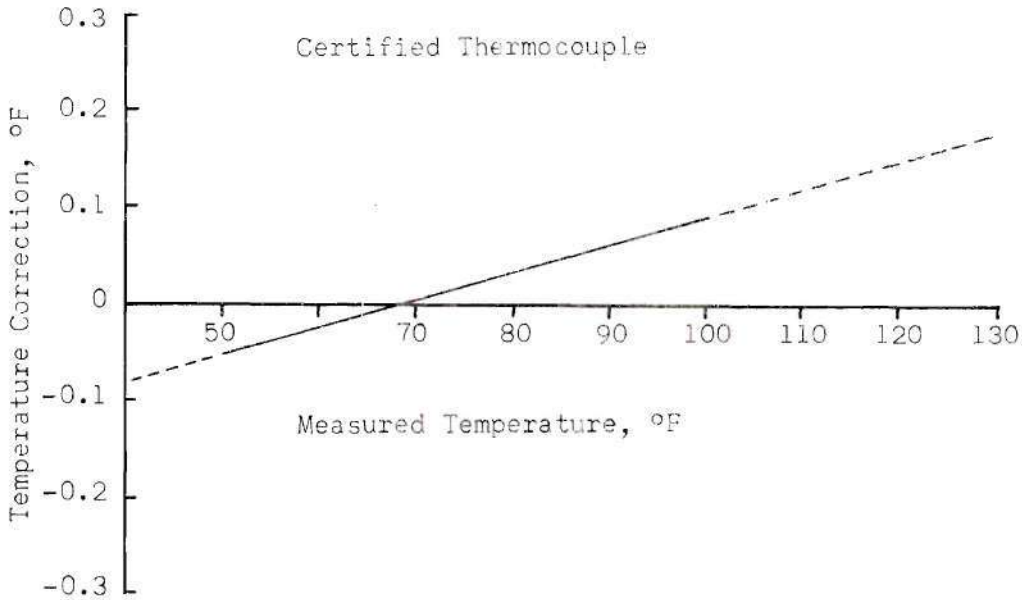

Figure A-3. Calibration Curve for Certified Thermocouple.

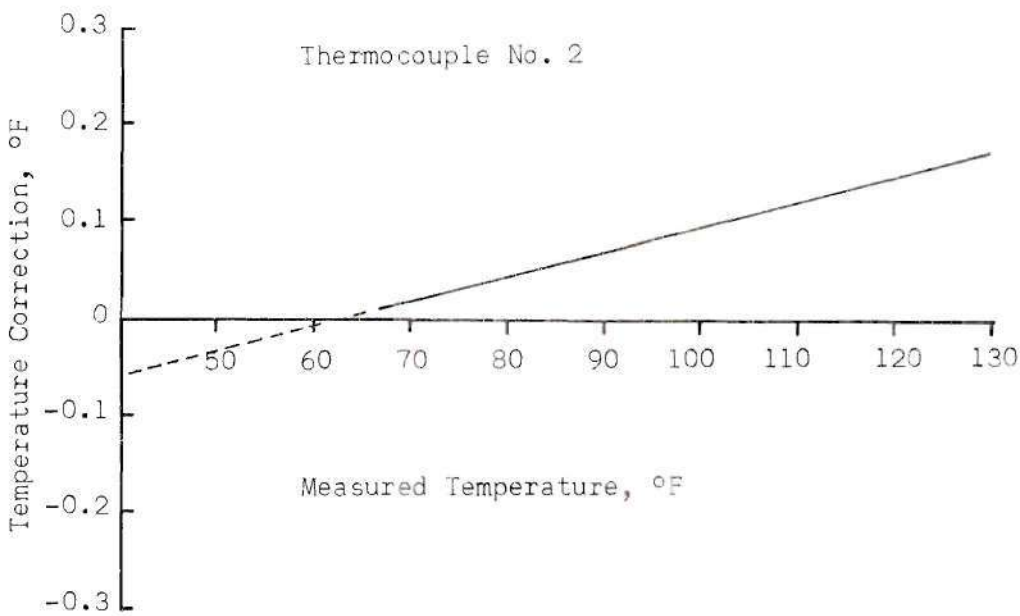

Figure A-4. Calibration Curve for Thermocouple No. 2.

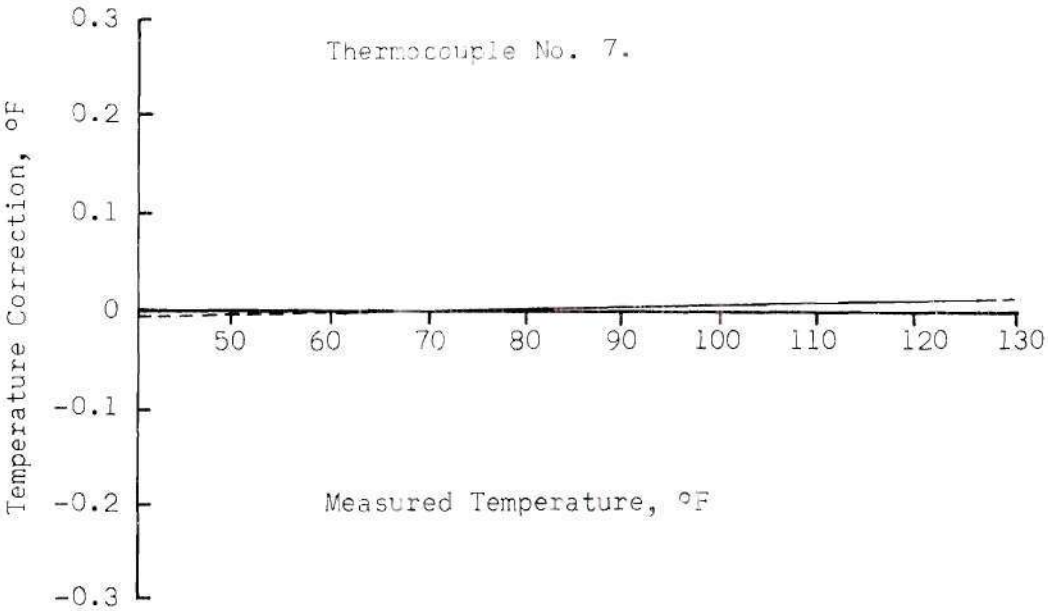

Figure A-5. Calibration Curve for Thermocouple No. 7.

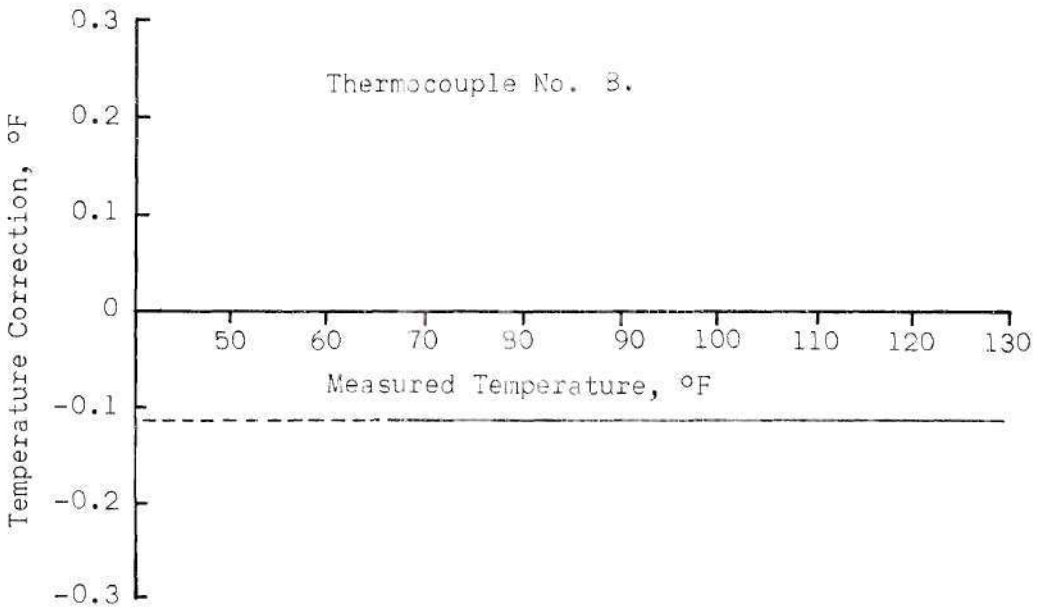

Figure A-6. Calibration Curve for Thermocouple No. 8.

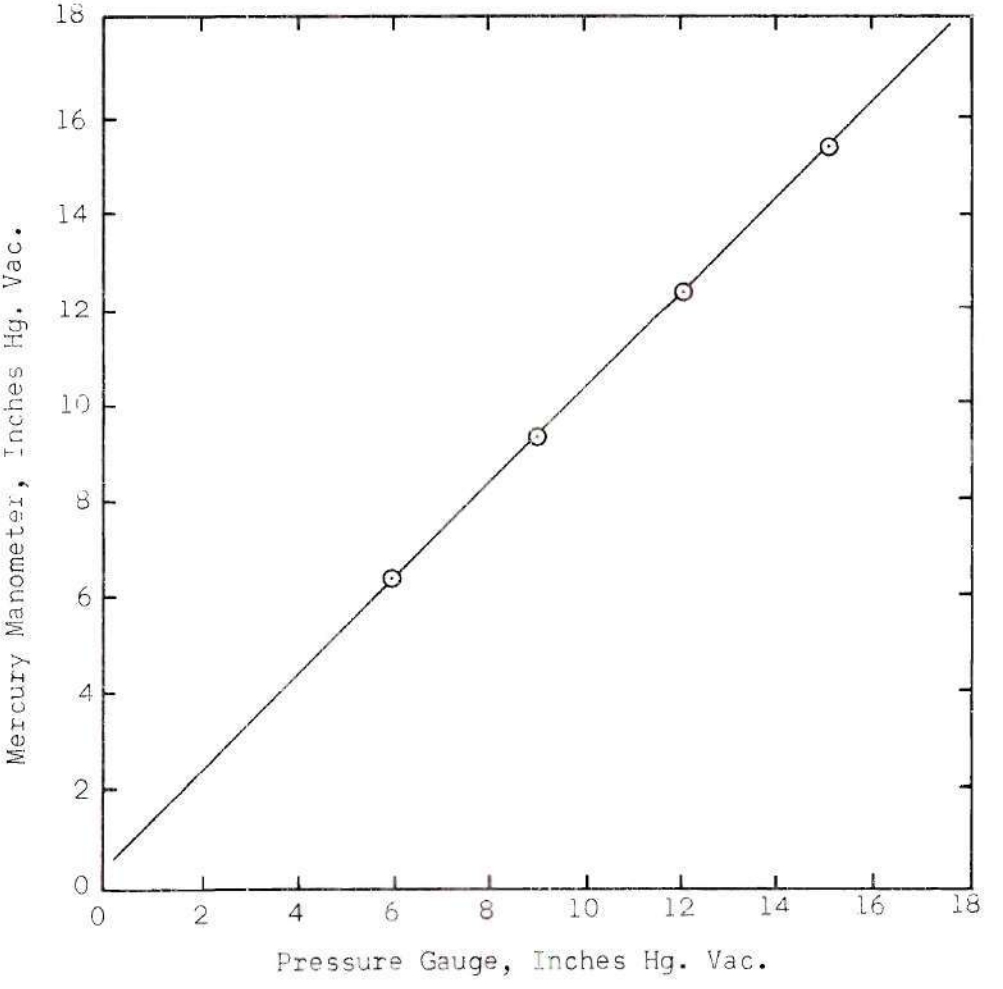

Figure A-7. Calibration Curve for Pressure Gauge.

Error Analysis

Electric Field

The voltage difference between the two test voltage probes was measured with a Moseley 7100BM Strip Chart Recorder with a 17501A input module having an accuracy of better than ±0.2 per cent of full scale. The strip chart recorder was calibrated with a Fluke 405B High Voltage DC Power Supply with an accuracy of ±0.25 per cent or 250 millivolts. The voltage probe locations were known to within about ±1/4 millimeter or within ±3 per cent. The electric field was calculated from the voltage measurement and the probe separation distance from the equation $E = V/\ell$. The electric field is estimated to have an accuracy of about ±5 per cent.

Current Density

The total current passing through the test section was obtained by measuring the voltage drop across an Esterline 150 ampere/100 millivolt Shunt with a Moseley 7100BM Strip Chart Recorder with a 17501A input module having an accuracy of better than ±0.2 per cent of full scale. The strip chart recorder was calibrated with a Leeds and Northrup Millivolt Potentiometer No. 8686. The diameter of the test section was known to within ±1/4 millimeter or within ±2 per cent. The current density was calculated from the measured total current and the cross-sectional area of the test section from the equation $j=I/A$. The current density is estimated to have an accuracy of about ±5 per cent. The calculation of current density assumes no radial variation of current density across the test section; however, the discharge was visually observed to almost completely fill the section between the test electrodes.

Electrical Conductivity

The average electrical conductivity was calculated from the average electric field and the average current density according to the equation $\sigma = j/E$. The errors in current density and electric field also appear in the electrical conductivity. Observe; however, that an error in the current density will only shift the data points along the conductivity curve since the slope is about unity, while an error in the electric field will cause the data to deviate from the conductivity curve. The average electrical conductivity is estimated to have an accuracy of about ±7 per cent.

Gas Temperature

The gas temperature was obtained from measurements of the temperature of a tungsten wire probe immersed in the gas stream with a Leeds and Northrup optical pyrometer. The pyrometer was calibrated with a Mole-Richardson Type 2731 Molarc Lamp according to the procedure given in the Appendix. The Molarc Lamp provided a source temperature of 3803 ± 20°K. The filter glasses used for the calibration were tested by the National Bureau of Standards with the following results:

Table 3. NBS Calibration of Filter Glasses for Molarc Lamp

Filter	Nominal T_{app}	"A"($K^{-1} \times 10^{-6}$)	Per Cent Maximum Uncertainty
1300-45	1300°K	501	3/4
1800-45	1800°K	286	1
2300-45	2300°K	171	1

where the "A" in the table is defined by the following equation:

$$\text{"A"} = \frac{1}{T_{app}(K)} - \frac{1}{T_{source}(K)}$$

The results of the pyrometer calibration are given in Table 2 of the Appendix. Based on the above, it is estimated that the gas temperature has an accuracy of within ±40°K. A systematic 40°K error in gas temperature would shift the electrical conductivity curve by about 3 to 6 per cent.

Seeding Fraction

The potassium seeding fraction was calculated from the following equation:

$$\frac{n_K}{n_A} = \frac{\dot{m}_K \tilde{M}_A}{\dot{m}_A \tilde{M}_K} \simeq \frac{\dot{m}_K}{\dot{m}_A}$$

Thus, the accuracy of the seeding fraction depends on the accuracy of the potassium and argon flow rate measurements. The argon flow rate was measured with a calibrated thin plate orifice with an accuracy of ±3 per cent of full scale; therefore, the argon flow rate should be accurate to about ±6 per cent.

The potassium flow rate was obtained by measuring the feed rate of the positive displacement feed mechanism. Potassium temperature was maintained at about 90 ± 10°C. This temperature uncertainty leads to negligible errors in the density of liquid potassium. Errors due to nonuniformity of screw threads and motor speed are estimated to be within

±3 per cent. Combining these effects leads to an accuracy in seed fraction of about ±7 per cent which would shift the electrical conductivity curves about ±3 per cent.

Gas Pressure

The gas pressure was measured by a Crosby vacuum-pressure meter with a range of from 30 inches of mercury vacuum to 30 psig. The meter was calibrated with a mercury manometer. Due to variations in pressure which occurred during a run, the gas pressure is estimated to have an accuracy of about ±1 inch of mercury.

Potassium Loading Procedure

1. Place a pan of kerosene on a heating unit and heat to a temperature of about 180°F. Maintain this temperature for about 15 minutes to remove the air from the kerosene.
2. Submerge a 10 gram ampule of potassium under the kerosene and break the end of the glass ampule.
3. Apply a thin coating of Dow Corning silicone high vacuum grease to the piston of a 10 cc Luer-Lok syringe to provide a good seal.
4. Fit the syringe with a 4 inch long 20 gauge needle and submerge under the kerosene. Fill the syringe and needle with kerosene and then empty it to remove any air in the syringe and needle.
5. As soon as the syringe has reached the temperature of the kerosene bath, push the needle below the surface of the potassium metal and pull the desired amount of potassium into the syringe.
6. While still submerged under kerosene, remove the 4 inch long needle and replace it with a 1 inch long 24 gauge needle. The loaded syringe is now ready to be placed in the potassium syringe holder.

```
      BURROUGHS B-5500 ALGOL COMPILER LEVEL    9      FRIDAY,    7/12/68,   5:24 PM.

%USER= B179981.  BIN 0894                                                          0000
%COMPILE BIN0894/CONDRAD ALGOL          .03S800015   *0894 DOWDY M W               0000
%PROCESS=0020;10=0015;ALGOL   PROCESS=15;ALGOL   10=15.                            0000
%DATA.                                                                             0000
%DATA CAMWD .                                                                      0000
BEGIN                                                                              0000
                                                        START OF SEGMENT **********  2
LABEL    L1,L2                                                        ;            0000
         INTEGER I,J,K                                                ;            0000
         REAL C, C1,C2,C3,C4,C5,C6,F,TM,TC,C7,EA,EK,RHO,                           0000
         A1,A2,A3,A4,A5,A6,A7,B1,B2,NKO,NAO,GR1,GR2,G1,G2,QRAD        ;            0000
         ARRAY QA,QK,TE[1:86],TA[1:6],P[1:7],SIGMA,NE,CUR,ETAO,                    0000
         ETAI[1:7,1:86,1:6]                                           ;            0007
LIST     DATA(FOR J=1 STEP 1 UNTIL 86 DO QA[J], FOR K=1 STEP 1 UNTIL 86            0009
         DO QK[K])                                                    ;            0016
LIST     ANS(SIGMA[I,J,K],NE[I,J,K],CUR[I,J,K],TE[J],TA[K],P[I],                   0024
         ETAO[I,J,K]ETAI[I,J,K])                                      ;            0045
FILE IN  CAMWD (2,10)                                                 ;            0057
FILE OUT PIMWD 6(2,15)                                                ;            0061
FORMAT OUT TITLE(X8,"SIGMA",X7, "NE",X12,"CURRENT",X11,"TE",X8,"TA",X6,            0064
                                                        START OF SEGMENT **********  3
         "P",X11,"ETAO",X8,"ETAI"),FMT2(X5,F10.1,2E15.4,2F10.0,3E12.4),            0064
         FMT(/"RUN TIME=",F9.2,"SECONDS"/)                            ;            0064
         WRITE(PIMWD[NO])                                             ;            0064
                                                      3 IS   38 LONG, NEXT SEG  2
         READ(CAMWD,/,DATA)                                           ;            0066
         WRITE(PIMWD,TITLE)                                           ;            0071
         A1=1.46x1@-11                                                ;            0074
         A2=1.88x1@4                                                  ;            0075
         A3=1.61x1@7                                                  ;            0076
         A4=2.26x1@7                                                  ;            0078
         A5=3.98x1@-21                                                ;            0079
         A6=3.80x1@-21                                                ;            0080
         A7=3.0                                                       ;            0081
         B1=1.4                                                       ;            0082
```

```
          B2=0.7                                                                ;  0083
          C1=2.12936x1@14                                                       ;  0084
          C2=65.3                                                               ;  0085
          C3=1.23843x1@07                                                       ;  0086
          C4=1.79984x1@14                                                       ;  0087
          C5=5.03671x1@4                                                        ;  0088
          C6=8.10630x1@-36                                                      ;  0089
          C7=1.82883x1@5                                                        ;  0091
          F=0.004                                                               ;  0092
          C=1.3804x1@-23                                                        ;  0093
          TM=TIME(2)                                                            ;  0094
          FOR I=1 STEP 1 UNTIL 7 DO                                             0095
BEGIN     P[I]=3.0396x1@4+1.0132x1@4xI                                          ;  0123
          FOR K=1 STEP 1 UNTIL 6 DO                                             0125
BEGIN     TA[K]=1000+500xK                                                      ;  0131
          FOR J=K STEP 1 UNTIL 86 DO                                            0132
BEGIN     TE[J]=1400+100xJ                                                      ;  0135
          EA=((C4xTE[J])*1.5)xEXP(-C7/TE[J])                                    ;  0136
          EK=((C4xTE[J])*1.5)xEXP(-C5/TE[J])                                    ;  0143
          RHO=0.0                                                               ;  0149
L1:       NE[I,J,K]=-EK/2+SQRT((EK*2)/4+(P[I]xFx(1+RHO)xEK)/((1+F)xCx           0151
          TA[K]))                                                               ;  0162
          IF ABS(RHO-(EAx(EK+NE[I,J,K]))/(FxEKx(EA+NE[I,J,K])))<0.01 THEN       0164
          GO TO L2                                                              ;  0175
          RHO=(EAx(EK+NE[I,J,K]))/(FxEKx(EA+NE[I,J,K]))                         ;  0176
          GO TO L1                                                              ;  0186
L2:       ETAO[I,J,K]=((C1x(TE[J]*0.5)xP[I])/((1+F)xTA[K]))x(QA[J]/             0187
          (NE[I,J,K]+EA)+FxQK[J]/(NE[I,J,K]+EK))                                ;  0202
          ETAI[I,J,K]=(C2/(TE[J]*1.5))xLN(C3x(TE[J]*1.5)/(SQRT(                 0212
          NE[I,J,K])))                                                          ;  0224
          SIGMA[I,J,K]=1/(ETAO[I,J,K]+ETAI[I,J,K])                              ;  0228
          NKO=(P[I]xFx(NE[I,J,K]/(NE[I,J,K]+EK)))/((1+F)xCxTA[K]x               0240
          (1+A7xEXP(-A2/TE[J])))                                                ;  0253
          NAO=(P[I]x(NE[I,J,K]/(NE[I,J,K]+EA)))/((1+F)xCxTA[K])                 ;  0256
          GR1=1+A5x(NKO+NAO)x(TA[K]*0.5)                                        ;  0269
          GR2=1+A6x(NKO+NAO)x(TA[K]*0.5)                                        ;  0274
          G1=A3xSQRT(GR1/NKO)                                                   ;  0279
```

```
        G2=A4xSQRT(GR2/NKO)                                          ;          0282
        QRAD=A1xNKOx(B1xG1+B2xG2)xEXP(-A2/TE[J])                     ;          0284
        CUR[I,J,K]=SQRT((C6x(NE[I,J,K])*2)x(TE[J]-TA[K])+            ;          0290
        QRADxSIGMA[I,J,K]                                            ;          0301
        WRITE(PTMWD,FMT2,ANS)                                        ;          0306
END                                                                  ;          0313
END                                                                  ;          0313
END                                                                  ;          0315
        TC=(TIME(2)-TM)/60                                           ;          0317
        WRITE(PTMWD,FMT,TC)                                          ;          0321
        END.                                                                    0330
                                                          2 IS 333 LONG, NEXT SEG   1

EXP IS SEGMENT NUMBER 0004,PRT ADDRESS IS 0111
LN IS SEGMENT NUMBER 0005,PRT ADDRESS IS 0110
SQRT IS SEGMENT NUMBER 0006,PRT ADDRESS IS 0113
OUTPUT(W) IS SEGMENT NUMBER 0007,PRT ADDRESS IS 0107
BLOCK CONTROL IS SEGMENT NUMBER 0008,PRT ADDRESS IS 0005
INPUT(W) IS SEGMENT NUMBER 0009,PRT ADDRESS IS 0106
X TO THE I IS SEGMENT NUMBER 0010,PRT ADDRESS IS )LL+
ALGOL WRITE   IS SEGMENT NUMBER 0011,PRT ADDRESS IS 0014
ALGOL READ    IS SEGMENT NUMBER 0012,PRT ADDRESS IS 0015
ALGOL SELECT  IS SEGMENT NUMBER 0013,PRT ADDRESS IS 0016
                                                          1 IS   2 LONG, NEXT SEG  0
                                                         14 IS  69 LONG, NEXT SEG  0

NUMBER OF ERRORS DETECTED =  0.  COMPILATION TIME =   11 SECONDS.
PRT SIZE =  77; TOTAL SEGMENT SIZE =  442 WORDS; DISK SIZE = 24 SEGS; NO. PGM. SEGS =  14
ESTIMATED CORE STORAGE REQUIREMENT = 6165 WORDS.
```

LITERATURE CITED

1. J. L. Kerrebrock, "Conduction in gases with elevated electron temperature," Engineering Aspects of Magnetohydrodynamics (Columbia University Press, New York, 1962), 327-346.

2. F. Robben, "Nonequilibrium ionization in a magnetohydrodynamic generator," Physics of Fluids 5, 1308 (1962).

3. W. Westendorp, C. Bishop, H. Hurwitz, L. Goldman and D. Ben-Daniel, "Nonthermal ionization in transient helium-cesium discharges," Physics of Fluids 4, 786-787 (1961).

4. D. BenDaniel and C. Bishop, "Nonequilibrium ionization in a high-pressure cesium-helium transient discharge," Physics of Fluids 6, 300 (1963).

5. H. Hurwitz, G. W. Sutton and S. Tamor, "Electron heating in magnetohydrodynamic power generators," American Rocket Society Journal 32, 1237 (1962).

6. J. L. Kerrebrock, "Magnetohydrodynamic generators with nonequilibrium ionization," American Institute of Aeronautics and Astronautics Journal 3, 591 (1965).

7. J. L. Kerrebrock, "Nonequilibrium ionization due to electron heating: I. theory," AIAA Journal 2, 1072 (1964).

8. J. Kerrebrock and M. Hoffman, "Nonequilibrium ionization due to electron heating: II. experiments," AIAA Journal 2, 1072 (1964).

9. R. Goldstein, J. K. Richmond and G. C. Oates, "Electrical conductivity measurements in a Faraday accelerator," Boeing Scientific Research Laboratories Document D1-82-0486 (1965).

10. F. C. Halstead and E. L. Larson, "Experimental determination of the electrical conductivity of noble gas-alkali metal plasmas," M.S. Thesis, Massachusetts Institute of Technology (1963).

11. S. C. Brown, Basic Data of Plasma Physics, (John Wiley and Sons, Inc., New York, 1959).

12. A. E. Sheindlin, V. A. Batenin and E. I. Asinovsky, "Experimental investigation of nonequilibrium ionization in a mixture of argon and potassium," Magnetohydrodynamic Electrical Power Generation (European Nuclear Energy Agency and Organization for Economic Cooperation, Paris, 1964).

13. E. E. Zukoski, T. A. Cool and E. G. Gibson, "Experiments concerning nonequilibrium conductivity in a seeded plasma," AIAA Journal 2, 1410 (1964).

14. E. E. Zukoski and T. A. Cool, "Nonequilibrium electrical conductivity measurements in argon and helium seeded plasmas," AIAA Journal 3, 370 (1965).

15. T. A. Cool and E. E. Zukoski, "Recombination, ionization, and nonequilibrium electrical conductivity in seeded plasmas," Phys. Fluids 9, 780 (1966).

16. S. V. Shelton and W. O. Carlson, "Variable collision cross-section effects on electrical conductivity," AIAA Journal 4, No. 9, Sept. 1966, pp. 1676-1677.

17. J. Bernard, E. Labois, P. Ricateau and P. Zettwoog, "Conductivite electrique des plasmas argon, cesium pour conversion MHD," Plasma Physics, 9, 1967, pp. 193-207.

18. T. F. Morse, "Energy and momentum exchange between non-equipartition gases," Phys. Fluids 6, 1420 (1963).

19. S. C. Lin, E. L. Resler and A. Kantrowitz, "Electrical conductivity of highly ionized argon produced by shock waves," Journal of Applied Physics 26, 95 (1955).

20. L. Spitzer Jr., and R. Harm, "Transport phenomena in a completely ionized gas," Physics Reviews 89, 997 (1953).

21. C. H. Kruger and J. R. Viegas, "Influence of the Ramsauer effect on nonequilibrium electron temperature," Phys. Fluids 7, 1879 (1964).

22. M. A. Lutz, "Radiant energy loss from a cesium-argon plasma to an infinite plane-parallel enclosure," Avco-Everett Research Rept. 175,BSD-TDR-64-6 (1963).

23. T. Holstein, "Imprisonment of resonance radiation in gases, II," Phys. Rev. 83, 1159-1168 (1951).

24. A. C. G. Mitchell and M. W. Zemansky, Resonance Radiation and Excited Atoms (Cambridge U. Press, London, 1934).

25. F. W. Hofmann and H. Kohn, "Optical cross-section of resonance lines emitted by flames under conditions of partial thermal ionization," Journal of Optical Society of America 51, 512 (1961).

26. N. K. Chaney, V. C. Hamister and S. W. Glass, "Properties of carbon at arc temperatures," Trans. of American Electrochemical Society 67, 107 (1935).

VITA

Mack Wayne Dowdy was born in Pitts, Georgia, on 25 August 1938. He is the son of Mack and Essie Mae Dowdy. In June of 1960 he was married to Eleanor Delores Robinson of Rochelle, Georgia. He now has two daughters, Kathy and Linda, and a son, Richard.

He attended public school in Pitts, Georgia and was graduated in 1956. He received the Bachelor of Mechanical Engineering Degree from the Georgia Institute of Technology in June of 1960. He obtained the degree Master of Science in Mechanical Engineering from the Ohio State University in December of 1961.

Following the Master of Science Degree, he served two years as an officer in the United States Army, being assigned to the Jet Propulsion Laboratory in Pasadena, California as a research engineer.

He returned to the Georgia Institute of Technology in January of 1964 to enter graduate school.